



HAL
open science

Ice on Noachian and Hesperian Mars: Atmospheric, Surface, and Subsurface Processes

Anna Grau Galofre, Jérémie Lasue, Kat Scanlon

► **To cite this version:**

Anna Grau Galofre, Jérémie Lasue, Kat Scanlon. Ice on Noachian and Hesperian Mars: Atmospheric, Surface, and Subsurface Processes. *Ices in the Solar System*, In press. hal-04204657

HAL Id: hal-04204657

<https://hal.science/hal-04204657>

Submitted on 12 Sep 2023

HAL is a multi-disciplinary open access archive for the deposit and dissemination of scientific research documents, whether they are published or not. The documents may come from teaching and research institutions in France or abroad, or from public or private research centers.

L'archive ouverte pluridisciplinaire **HAL**, est destinée au dépôt et à la diffusion de documents scientifiques de niveau recherche, publiés ou non, émanant des établissements d'enseignement et de recherche français ou étrangers, des laboratoires publics ou privés.

24 **Abstract**

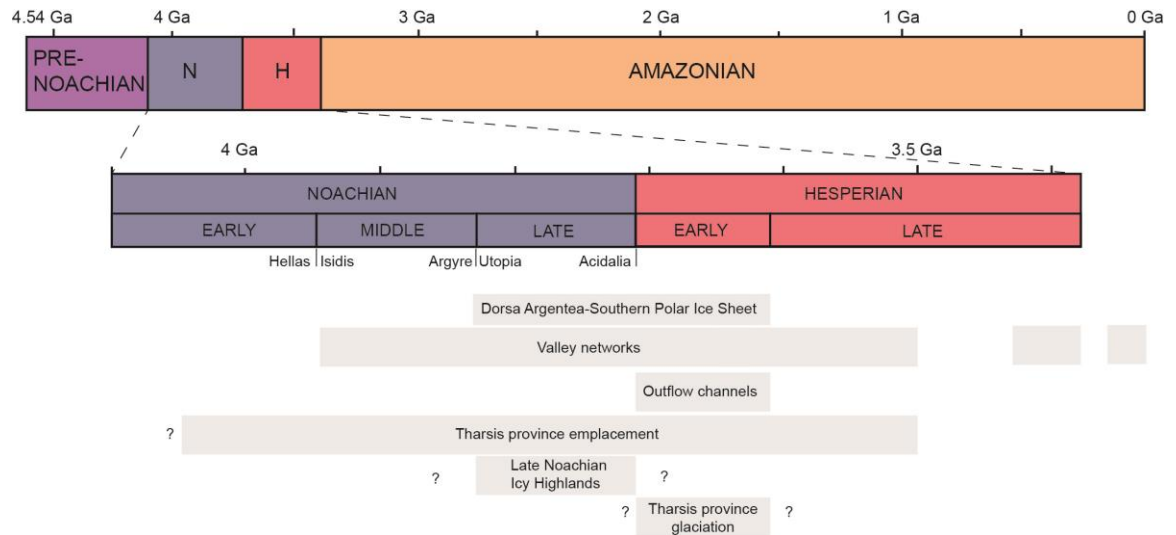
25 Much of the Noachian-Hesperian (i.e. > ~3.0 Ga) geology of Mars remains exposed
26 at the surface, providing a unique opportunity for insight into the early history of an Earth-
27 like planet. Water ice, an important component of present-day Martian geology, was even
28 more abundant in the ancient past. This chapter presents an integrated view of ice on early
29 Mars, discussing the spatial extent, glacio-geology, and climate implications of an early
30 Martian cryosphere, and discusses repercussions for the water budget and its fate that are
31 relevant to later stages of Mars' history (Koutnik et al., 2023). In this chapter, we review
32 the predicted distribution of surface ice under various early Mars climate scenarios,
33 compare these hypothetical ice sheets to the locations on Mars where geological evidence
34 of ancient glaciations has been described, and consider the extent to which valley networks
35 are consistent with an ice-related origin. Finally, we consider the sequestration of ice
36 beneath the surface of Mars as the climate cooled following the time of valley network
37 incision. The abundance of new data from Mars exploration by satellites and rovers in
38 recent decades, along with advances in climate modeling, has allowed for novel insights
39 about the role of ice on early Mars.

40

41 **I. Introduction**

42 Mars is a cold planet relative to Earth (mean global surface temperature of
43 approximately -65°C), located between Earth and the asteroid belt at 1.5 AU from the Sun.
44 The geological history of over 4.5 Ga (Figure 1) is better preserved on Mars than on Earth,
45 given a lack of plate tectonics and exceedingly slow erosion rates (Carr., 2007). With a
46 large water inventory (thought to have been even more significant in early periods of its

47 history; e.g. as observed in Carr and Head (2015), Lasue et al. (2013), Jakosky (2021)), a
 48 thicker early atmosphere, and chaotic obliquity/eccentricity variations throughout history
 49 (e.g., Baker., 2001, Laskar et al., 2004, Carr and Head, 2015, Wordsworth, 2016), Mars
 50 poses a fascinating case study for the evolution of ice on a terrestrial planet and its influence
 51 in shaping surface morphology.



52

53 Figure 1: Geologic timeline showing the three major divisions in Mars' history (Noachian,
 54 Hesperian, Amazonian), with focus on the 'early Mars' Noachian and Hesperian eras,
 55 described in this chapter. A summary of the most representative events, as well as the
 56 timing of major glacial episodes, is shown in the figure. Age boundaries presented follow
 57 the Neukum chronology system (Hartmann and Neukum, 2001).

58

59 The topography of Mars (Figure 2) is primarily a product of volcanism and impact

60 cratering (e.g. Smith et al., 2001), rather than of plate tectonics as on Earth (e.g. Black et

61 al., 2017). In the absence of a sea level, elevations for points on Mars are given relative to

62 a reference equipotential surface (Smith et al., 2001). The dichotomy boundary, coinciding

63 roughly with the 0 m reference elevation, divides the planet into lowland plains in most of

64 the northern hemisphere and crater-studded highlands in the southern hemisphere. The

65 crustal dichotomy is generally thought to be the result of a large impact or series of impacts

66 in the early Noachian era (Marinova et al., 2008, Pan et al., 2017), but a mantle plume

67 hypothesis is also plausible (e.g. Šrámek and Zhong., 2012, Citron et al., 2018). The
 68 equatorial Tharsis bulge (e.g. Phillips et al., 2001, Bouley et al., 2016) is a volcanic
 69 construct with elevation up to +7 km and upon which the Tharsis Montes volcanoes stand
 70 up to +18 km. Two large impact basins, Hellas and Argyre, occur in the southern
 71 hemisphere (e.g. Hiesinger and Head, 2002, Bernhardt et al., 2016). The floor of Hellas
 72 basin, with elevations ~5 – 8 km below the reference surface, is the lowest point on the
 73 planet.



74

75 **Figure 2:** Geography of Mars as referenced in this chapter. THEMIS daytime IR 100 m
 76 global basemap (Edwards et al., 2011) with Mars Orbiter Laser Altimeter (MOLA)
 77 elevation color overlay (Smith et al., 2003). Valley networks as mapped by Hynek et al.
 78 (2010) are shown in blue-green.

79

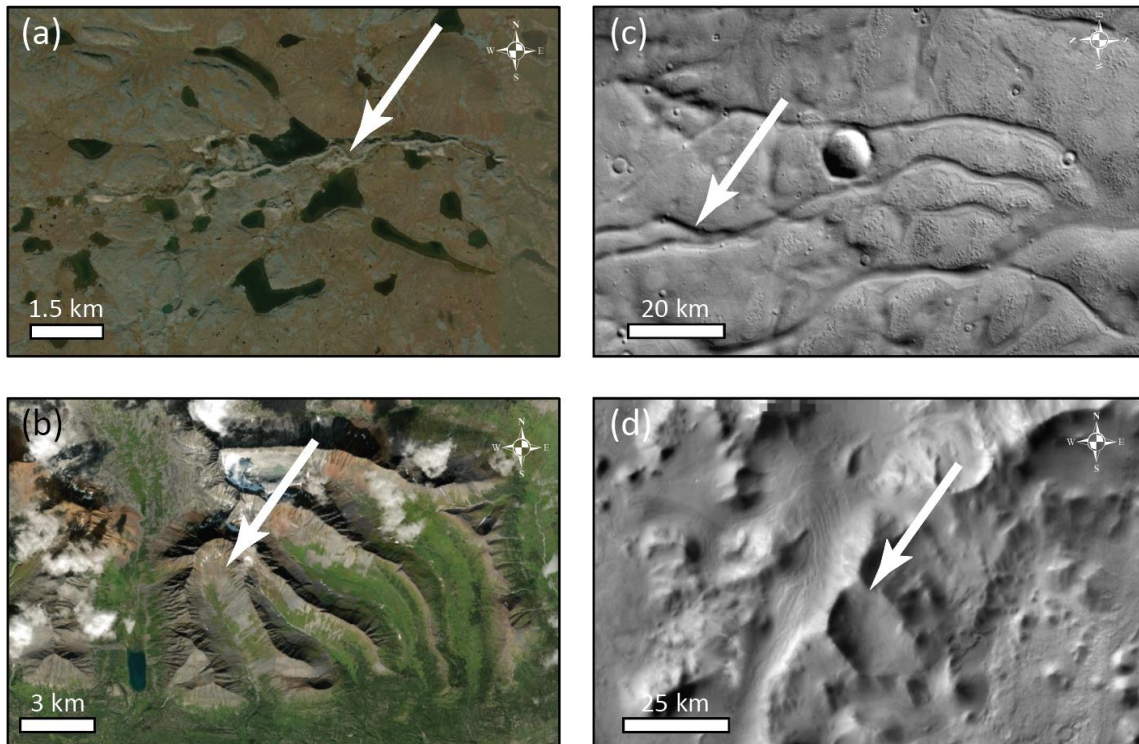
80 This chapter explores the glacio-geological history of early Mars, including
 81 atmospheric, glacial and deep cryospheric processes. We use the term “glaciation” to
 82 describe the suite of processes involving the accumulation of surface crystalline ice. We
 83 use the term “deep cryosphere” to describe ice and ice-rich substrate located below the

84 depth of direct interaction with the atmosphere. The Noachian and Hesperian eras are
85 thought to have been characterized by a thicker atmosphere, lower insolation, and a larger
86 water budget than present day (Wordsworth, 2016, Carr and Head, 2015). Characteristics
87 such as a lower surface gravity than Earth, a north-south topographic dichotomy, and
88 chaotic obliquity/eccentricity variations have remained throughout Mars' history. To
89 describe the current knowledge of glacial and ground ice on early Mars, we consider three
90 questions:

91 *1. How was ice distributed at the surface of Mars in the Noachian and Hesperian?*

92 In the thin present-day Martian atmosphere, the ground surface temperature at any point
93 on the planet is determined almost entirely by the sunlight absorbed at that point (e.g. Read
94 and Lewis, 2004). As such, at the present-day spin-axis obliquity of $\sim 25^\circ$, surface ice is
95 stable only at the north and south poles. If early Mars had a higher surface pressure, as
96 geomorphologic, geochemical, isotopic, and escape rate evidence suggest it did (e.g.
97 Manga et al., 2012, Kite et al., 2014, Bristow et al., 2017, Warren et al., 2019, Kite, 2019,
98 Jakosky et al., 2021), the greater heat capacity of the atmosphere would allow much more
99 heat exchange between the atmosphere and the surface (or the greater greenhouse effect
100 would result in more longwave radiation to the surface from the atmosphere; cf. Fan et al.,
101 2022). In this case, ground surface temperatures would decrease with altitude as
102 atmospheric temperatures do, and ice would be expected to accumulate at high altitudes
103 (Forget et al., 2013, Wordsworth et al., 2013). We will describe the scenarios currently
104 under study by climate modelers, and the geologic evidence for ice in Noachian and
105 Hesperian terrains (Figure 3).

106



107
 108 **Figure 3:** Example terrestrial analogue features (a,b) and martian equivalent landforms
 109 (c,d). (a) Terrestrial esker centered around 66.21N, 111.78W (Kugluktuk land, NU,
 110 Canada). (b) Glacial cirques at 62.64N, 128.57W (Nááts'ihch'oh National Park Reserve,
 111 AK, United States). Credit: Esri/Maxar/ArcGIS. (c) Dorsa Argentea eskers, centered
 112 around 76.81S, 317.9E. Credit: CTX/MSSS/NASA. (d) Putative glacial cirques in the
 113 Charitum Montes, southern Argyre rim (center: 55.41S, 307.8E). Credit:
 114 THEMIS/ASU/JPL-Caltech/NASA.

115
 116 *2. What fraction of observed fluvial geology on Mars is due to ice melt?* The crater
 117 lake systems and valley networks in the equatorial and southern highlands of Mars are
 118 generally agreed to have formed by the action of liquid water (e.g. Carr, 1995, et al., 1999,
 119 Gulick, 2001, Craddock and Howard, 2002, Hynek et al., 2010, Fassett and Head, 2008b,
 120 Goudge et al., 2015), but there is less consensus as to whether that water fell to the surface
 121 as rain or resulted from snow and/or ice melt. Some researchers have argued that the
 122 Martian valley networks and crater lakes could have been carved primarily by meltwater,
 123 either as snowmelt (e.g., Carr and Head, 2003, Wordsworth et al., 2015), as top-down
 124 melting from a hypothesized ice sheet covering the highlands (e.g., Fastook and Head,

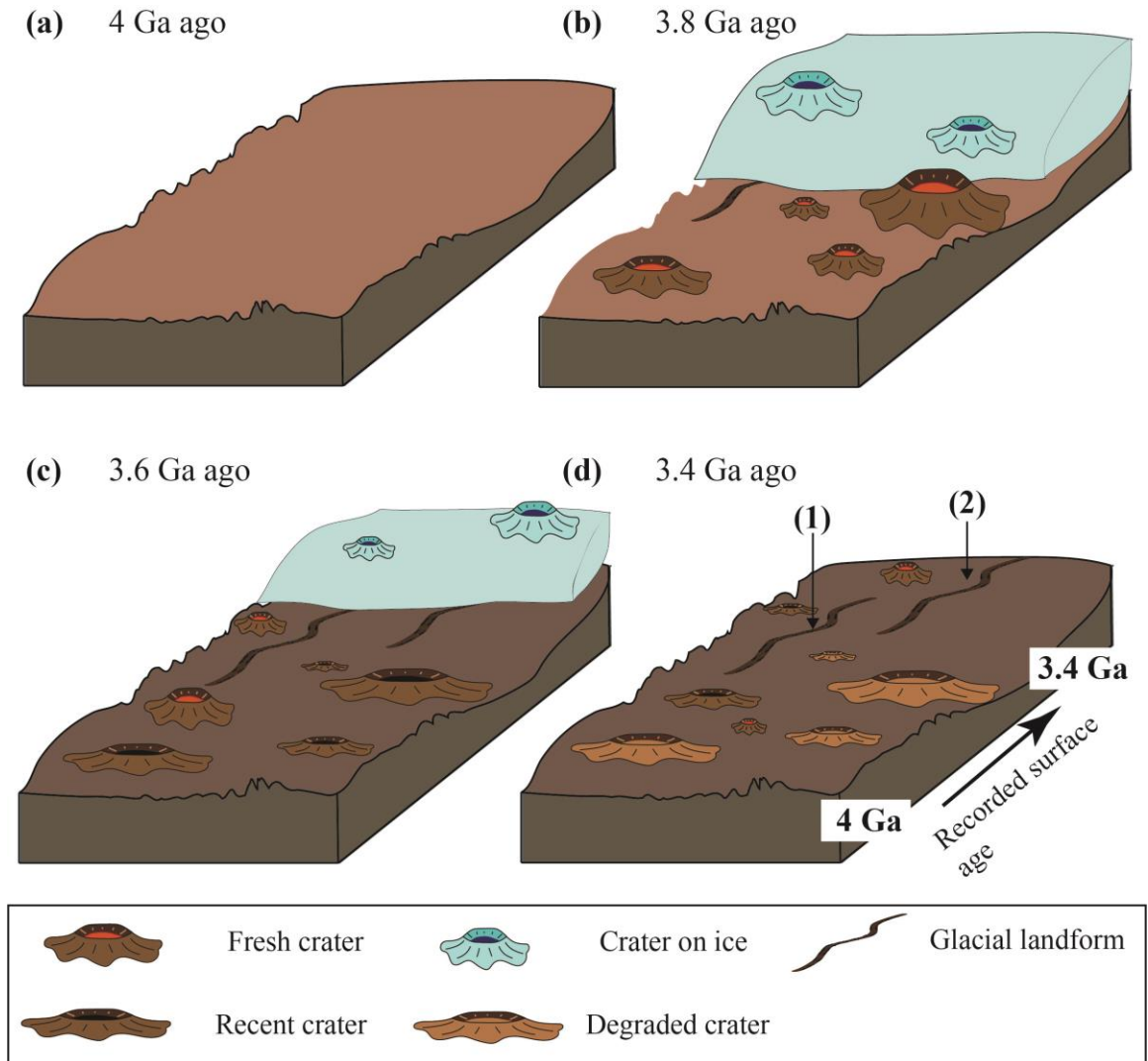
125 2015), or as subglacial channelized melt from a similar environment (e.g. Grau Galofre et
126 al., 2020a). Others hold that they indicate a relatively temperate climate in the Noachian-
127 Hesperian with rainfall and/or groundwater seepage (e.g., Carr, 1995, Gulick, 2001,
128 Craddock and Howard, 2002, Howard et al., 2005, Irwin et al., 2005, Hynek et al., 2010,
129 Irwin et al., 2011, Ramirez and Craddock, 2018, Kite, 2019). We will review the evidence
130 for both endmembers, and consider intermediate scenarios.

131 *3. How did the subsurface water inventory and cryosphere evolve with time, and*
132 *what is its effect on the global water inventory?* Finally, we consider the possibility of ice
133 beneath the surface of Mars, modeling the thickness and depth of the subsurface cryosphere
134 as a function of latitude, brine composition, and orbital parameters. We discuss the
135 proportion of the total Martian water inventory that could be confined in the subsurface
136 and the observational evidence on which these calculations are based. This informs the
137 availability of ice for processes on recent Mars (as discussed by Koutnik et al. (2023)).

138

139 To preface our in-depth discussion of early Mars glacial geology, we note that
140 precise dating of glacial and periglacial landscapes is not without controversy. In addition
141 to the broader uncertainties in dating the surface of Mars with impact crater size-frequency
142 distributions (e.g. Robbins et al., 2013), three problems arise with the dating of glacial
143 terrains on Mars. First, these techniques provide the modelled age of a terrain, not of
144 landforms within it, which can be much younger. Buffered crater counting methods, such
145 as those developed for valley networks and eskers (e.g., Fassett and Head, 2008a, Kress
146 and Head, 2015), provide more accurate constraints on the age of a landform than crater
147 counting of the underlying geology, but are not always feasible given the small areal extent

148 of individual landforms. Second, glacial landscapes formed in the Noachian and Hesperian
149 have undergone over 3 Ga of degradation, including crater gardening, mass wasting,
150 intermittent glacial/fluviol erosion, and mantling, among other processes. Therefore, the
151 interpretation of glacial landform assemblages as part of a group of the same age is further
152 hindered due to the different levels of degradation of individual features, including older
153 craters. The third issue involves the role of an ice cover in preventing smaller impacts from
154 penetrating to the surface. The decoupling of surface and atmosphere by an ice layer is
155 indeed a major issue for dating glacial landscapes even on Earth, where isotopic dating of
156 terrains provides ages of ice retreat and not erosion rates or dates of landform emplacement
157 (e.g., Balco et al., 2011 and references within). Modelled ages derived from crater counting
158 in regions with extensive ice cover may record the time-integrated effect of intermittent
159 surface cover, resulting in a crater counting age much younger than the true age of the
160 landscape due to ice cover filtering of smaller impacts. Furthermore, crater counting dates
161 would reflect the timing of ice retreat from a subglacial landform and not of subglacial
162 landform emplacement. This ice-crater filtering effect depends at least on ice sheet
163 thickness and projectile momentum upon impact, but concrete numbers require modelling
164 efforts that have not yet been performed for Mars, and are thus a necessary future line of
165 research.



166

167 **Figure 4:** Cartoon illustrating the issues of crater dating surface modification in ice-
 168 covered surfaces. Panel (a) shows an originally emplaced, pristine surface 4 Ga ago, aged
 169 4 Ga. Panel (b) corresponds to the same surface covered by an ice sheet at 3.8 Ga. Fresh
 170 craters on land and ice are shown, and a glacial landform (e.g., esker) emerges from under
 171 the ice. Panel (c) shows ice retreat 3.6 Ga ago, exposing more of the original landform and
 172 a second one. Fresh and recent craters are shown on land and ice. Panel (d) shows the final
 173 surface after ice retreat, at $t = 3.4$ Ga. Crater size distribution and density change from the
 174 surface that was always fully exposed, to that covered by an ice layer, yielding apparently
 175 different age dates. The emplacement ages of eskers (1) and (2) are unknown, whereas
 176 exposure ages are given by crater counting techniques.

177

178 Figure 4 illustrates these issues. The age of the surface is 4 Ga (panel a), but crater

179 dating landforms (1) and (2) yields at best ice retreat ages (3.6 Ga; panel c) and not the

180 time of emplacement (3.8 Ga; panel b). Degradation of craters and subsequent resurfacing

181 (represented by color changes; panel d) further complicates the dating of individual
182 landforms. Landforms (1) and (2) could have formed simultaneously under the ice sheet,
183 but their age dates according to crater counting techniques display 0.2 Ga of age difference,
184 due to the different exposure times. Similarly, any dating of glacial landforms will refer to
185 ‘exposure dates’ and not reflect the time of emplacement or formation. This challenge
186 becomes more acute if a surface has been influenced by multiple glacial cycles and/or
187 postglacial revision. Accurate dating of glacial landforms is a major unresolved issue in
188 early Mars glacial geomorphology.

189 **II. Question 1: How was ice distributed at the surface of Mars in the Noachian and** 190 **Hesperian?**

191 While the MAVEN mission confirmed that the inventory of water on early Mars
192 was five to twenty times larger than on present-day Mars (Jakosky, 2021), geologic
193 constraints on the atmospheric composition and pressure of Early Mars are few and
194 imprecise (Kite, 2019). However, climate hypotheses can also be tested by comparing the
195 observed locations of geologic features to the surface temperature patterns and distribution
196 of volatiles modeled by three-dimensional global climate models (GCMs) under various
197 paleoclimate scenarios. Most Early Mars 3D GCM studies thus far have focused on climate
198 conditions under which the valley networks could have formed (e.g. as mapped by Hynek
199 et al., 2010; Figure 2). Scenarios that have been considered in GCM studies fall into one
200 of three categories:

201 *Thick atmosphere, CO₂/H₂O only.* Researchers working with the Laboratoire de
202 Météorologie Dynamique (Forget et al., 2013, Wordsworth et al., 2013), MarsWRF
203 (Mischna et al., 2013), NCAR CAM-based (Urata and Toon, 2013), CCSR/NIES/FRCGC

204 (Kamada et al., 2020), and ROCKE-3D (Guzewich et al., 2021) GCMs found that in
205 simulated atmospheres with similar composition to present-day Mars but much greater CO₂
206 partial pressure, ice migrates over time to cold traps in the southern highlands, southern
207 polar regions, and the equatorial Tharsis bulge. In simulations where spin-axis obliquity is
208 varied (Wordsworth et al., 2013, Mischna et al., 2013), ice is most stable at the south pole
209 when obliquity is low ($\leq \sim 25^\circ$), and at Tharsis when it is high ($\geq \sim 42^\circ$).

210 *CO₂/H₂O with CH₄, H₂ and/or another effective greenhouse gas:* Since thick
211 CO₂/H₂O atmospheres can account for large quantities of ice migrating to the equatorial
212 locations where fluvial features are observed, but not the temperatures required to melt ice
213 or allow rainfall in those regions, subsequent GCM studies investigated the efficacy of
214 additional greenhouse gases. Sulfur dioxide, a favored candidate in earlier work given its
215 production in volcanic eruptions (e.g. Halevy et al., 2007, Johnson et al., 2008), was found
216 by more recent studies to produce only a small warming effect (Mischna et al., 2013,
217 Kerber et al., 2015). Theoretical calculations of collision-induced absorption (CIA) in CO₂-
218 CH₄ or CO₂-H₂ atmospheres (Ramirez et al., 2014, Wordsworth et al., 2017) showed that
219 1D models of the early Mars atmosphere are substantially warmer when the effect of CIA
220 between CO₂ and either CH₄ or H₂ is included in radiative transfer calculations. Later
221 laboratory measurements, extrapolated theoretically to a broad temperature range and
222 incorporated into a 1D climate model, determined that warming due to CO₂-CH₄ CIA is
223 not sufficient to bring the annual mean surface temperature of early Mars above freezing
224 for reasonable CO₂ surface pressure or CH₄ concentrations, but CO₂-H₂ CIA could
225 plausibly do so (Turbet et al., 2019, 2020, Godin et al., 2020).

226 In 3D simulations of an early Mars warm enough to experience significant rainfall,
227 whether due to an idealized “grey gas” whose absorptivity does not vary with wavelength
228 (Wordsworth et al., 2015) or CH₄ and H₂ (Kamada et al., 2020, Guzewich et al., 2021),
229 annual mean temperatures remain below freezing in the Tharsis plateau. In cooler but still
230 rainy climates, substantial ice accumulation also occurs at latitudes below 60° S (Kamada
231 et al., 2020).

232 In 3D GCM simulations of a warm early Mars at 25° or 42° obliquity and with
233 modern topography (Wordsworth et al., 2015, Kamada et al., 2020), the Margaritifer Sinus
234 region is dry due to a rain shadow east of Tharsis, despite being well-dissected by valleys
235 in reality. Recent work found much better correspondence between rainfall and valley
236 network drainage density, provided spin-axis obliquity is very low (0°; Guzewich et al.,
237 2021). While ice accumulation in the 0° obliquity warm early Mars scenario is not
238 described, snowfall maxima occur on Tharsis and in the southern polar highlands.

239 *CO₂/H₂O with an effective greenhouse gas and/or additional, non-atmospheric*
240 *factors:* In an alternative “true polar wander” scenario, Tharsis formed north of the equator
241 after most valley network incision had already occurred, and the spin axis of the planet
242 reoriented over tens of millions of years to position the Tharsis load at the equator (Bouley
243 et al., 2016). In simulations using pre-Tharsis topography and the corresponding spin axis
244 orientation, precipitation patterns closely resemble the observed distribution of valley
245 networks at a broader range of obliquities (Bouley et al., 2016, Guzewich et al., 2021), and
246 the lack of the Tharsis cold trap leaves more of the Martian water inventory available to
247 circulate as precipitation and runoff (Guzewich et al., 2021). Regions favorable for ice
248 accumulation in the CO₂-only true polar wander scenario are at the north paleo-pole in

249 Scandia Colles, the south paleo-pole in Malea Planum, and a band corresponding to the
250 paleo-equator (Bouley et al., 2016).

251 Mischna et al. (2013) simulated warming only by CO₂, SO₂ and H₂O, but found
252 that by prescribing a lower-than-current albedo—approximating that of unweathered basalt
253 or an ice-free ocean—in the northern lowlands, they could maintain surface temperatures
254 in Hellas and the lowlands above freezing for 30-70% of the year. In these scenarios,
255 Tharsis, the south pole, and much of Promethei Terra still remained below freezing year-
256 round. In the first early Mars GCM study featuring a coupled dynamical ocean model,
257 Schmidt et al. (2022) found that an ice-free ocean could remain stable on early Mars even
258 with global mean temperatures below 273 K due to heat transport within the ocean. In this
259 scenario, extensive surface ice was present from Alba Mons across Tharsis to Terra
260 Sirenum, at Elysium Mons, at the south pole, in the high terrain ringing Hellas, and along
261 the dichotomy boundary from Isidis to Arabia Terra.

262 Comparing the predictions of these models, several key areas emerge where model
263 predictions converge or diverge: Tharsis, the poles, and the highlands.

264 *The Tharsis rise:* Ice accumulation in Tharsis is a robust, recurring feature of early
265 Mars GCM simulations, but the search for evidence of early Martian glaciation in the
266 region is complicated by lava flows that have resurfaced the region in the Amazonian (e.g.
267 Werner, 2009). Direct morphological evidence of ancient ice in the Tharsis region is scant
268 at present. A Late Hesperian landform assemblage near the Oudemans crater has been
269 interpreted as glacial (Yin et al., 2021), and the “Northwestern Slope Valleys” (NSVs)
270 adjoining the Tharsis rise have been hypothesized to result from erosion by a late Noachian
271 – early Amazonian ice stream (Kite and Hindmarsh, 2007).

272 The Olympus Mons basal escarpment has been interpreted as evidence that the
273 volcano was constructed within an ice sheet (Hodges and Moore, 1979, Helgason, 1999,
274 Cassanelli and Head, 2019), but it is also plausible that Olympus Mons and its scarp formed
275 underwater (e.g. De Blasio, 2018, 2020) or that the scarp is a result of subaerial landslides
276 lubricated by ground ice (e.g. Lopes et al., 1980, Tanaka et al., 1985). Relatedly, the
277 distribution of regional faults and outflow channels indicate that the shape of the
278 Thaumasia Plateau southeast of Tharsis may be the result of gravity spreading enabled by
279 buried salts and ground ice (Montgomery et al., 2009).

280 Grooves and streamlined islands in Echus Chasma and Kasei Valles (Zealey, 2009,
281 Chapman et al., 2010, Neukum et al., 2010, Cassanelli and Head, 2019) are attributed to
282 voluminous floods originating from Tharsis in the late Noachian and early Hesperian.
283 Cassanelli et al. (2015), noting the Wordsworth et al. (2013) prediction of abundant water
284 ice in Tharsis and the capacity of ice cover to raise the melting isotherm in the underlying
285 cryosphere, found that basal melting of a 1500 m thick Tharsis ice sheet could only
286 recharge the aquifer with less than half the volume of water inferred to have carved the
287 smallest outflow channels. However, these calculations assumed a 224 K surface
288 temperature for the Tharsis region (Wordsworth et al., 2013); recharge volumes could be
289 much larger in a climate where Tharsis surface temperatures are closer to the freezing point
290 (Cassanelli et al., 2015). Subsequent GCM studies have shown that Tharsis, while
291 consistently below 273 K, can experience annual average temperatures tens of degrees
292 above 224 K in climate scenarios warm enough for rain near the equator (e.g. Guzewich et
293 al., 2021, Figures 5 and 16, Turbet et al., 2017).

294 *The highlands and the dichotomy boundary:* In discussions of a hypothetical cold
295 early Mars, the highlands glaciation predicted by GCMs is often idealized as a globally
296 uniform ice cover at every point on the surface at elevation above +1 km. However, it must
297 be emphasized that stable locations for surface ice depend not only on annual maximum,
298 minimum, and mean surface temperature (which themselves vary with total atmospheric
299 pressure, greenhouse gas composition, and orbital parameters including eccentricity and
300 spin-axis obliquity) but on wind patterns and, in the shorter term, the distribution of water
301 vapor sources. For example, in early Mars ice flow simulations where mass balance was
302 idealized as a function of elevation only (Fastook and Head, 2015), the ice inventory of
303 Mars was spread across the entire highlands; no basal melting occurred and flow velocities
304 were minimal. In simulations with the same ice flow model, ice inventories, and
305 comparable mean annual temperatures, but where mass balance was instead derived from
306 the spatially varying potential sublimation (Wordsworth et al., 2015) predicted by the LMD
307 MGCM, ice sheets were confined to smaller regions of the highlands, flow velocities were
308 greater, and basal temperatures were higher (Scanlon, 2016, Fastook et al., 2021). This is
309 especially important at Hellas and Argyre, where steeper slopes at the basin edges and
310 warmer temperatures at lower altitudes result in relatively fast modeled flow into the basin
311 and strong modeled basal melting within them, and could explain the prevalence of ancient,
312 potentially glacial or glaciofluvial features reported in the two basins (Banks et al., 2009,
313 Bernhardt et al., 2013, Dohm et al., 2015, Bernhardt et al., 2016, Weiss and Head, 2017,
314 Bernhardt et al., 2019).

315 Several collections of landforms along the dichotomy boundary have been
316 interpreted as glacial in origin. Large outflow channels located in Chryse Planitia have

317 bedforms consistent with ice sculpture (Lucchitta, 1983, 1982, 2001, Chapman et al., 2010a
318 and b), which could suggest that an ice stream occupied the canyons for an unknown period
319 of time. Features interpreted as eskers, drumlins, kettles, and glaciovolcanic constructs are
320 present where the channels meet the lowlands (Martinez-Alonso et al., 2011). The Isidis
321 basin features numerous late Hesperian to early Amazonian landforms that resemble
322 terrestrial assemblages of moraines, kettle holes, eskers, tunnel valleys, and other glacial
323 features (e.g. Ivanov et al., 2012, Erkeling et al., 2014, Guidat et al., 2015, Souček et al.,
324 2015), as well as evidence for damming of a ~3.4 Ga lava flow by kilometers-thick ice
325 (Matherne et al., 2020). Ice sheet simulations of the Isidis basin closely replicate the flow
326 lines inferred from the orientation of hypothesized glacial landforms and suggest that the
327 region's characteristic ~3 Ga "thumbprint terrain" is a field of ribbed moraines resulting
328 from a ring of basal melting between the center and edges of the ice sheet (Souček et al.,
329 2015).

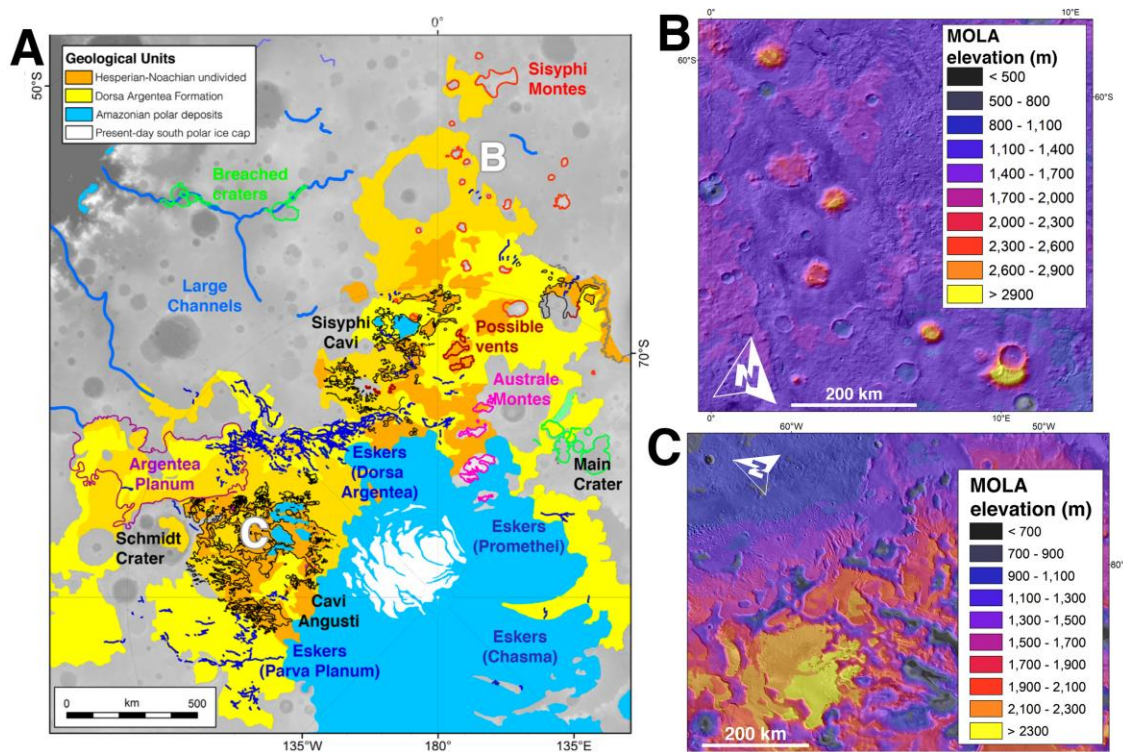
330 Terra Sabaea, an elevated region of the equatorial highlands northwest of Hellas
331 which is robustly glaciated in GCM simulations, is the site of several proposed valley
332 networks related to ice melt. Numerous anabranching inverted channels in an unnamed
333 Noachian crater in Terra Sabaea (Irwin et al., 2018, Boatwright and Head, 2021) originate
334 beneath upslope-facing scarps and crater wall alcoves and terminate in a basin with no
335 outlet or erosional inlet channels. Boatwright and Head (2021) argued that their distribution
336 is most consistent with an origin by top-down melting of a cold-based glacier whose
337 terminal moraines formed the present-day scarps. Bouquety et al. (2019, 2020) found that
338 late Noachian valleys in Terra Sabaea at elevations between +1 km and +3 km have short
339 length-to-width ratios and U-shaped cross-sectional profiles, and in many cases originate

340 from cirques, consistent with glacial erosion. Lower-altitude valleys are more frequently
341 V-shaped and do not head in cirques, and are hypothesized to originate from the melting
342 of a ~6200 km² ice cap on the plateau (Bouquety et al., 2020).

343 Another approach to the question is through statistical analysis of crater degradation
344 and other attributes. Weiss and Head (2015) suggested that many of the attributes of
345 degraded Noachian craters that have been attributed to rainfall could instead be a
346 consequence of impacts into ice, and suggested that the greater frequency of craters with
347 sharp rims and preserved ejecta at high altitudes (Craddock and Maxwell, 1993) could be
348 the result of protection by overlying cold-based ice sheets. A later study (Archer et al.,
349 2021) found that the degradation state of impact craters does not significantly differ above
350 and below 1 km elevation, i.e. within or outside of an idealized uniform highlands ice sheet,
351 but ongoing tests for differences in crater preservation across the highlands should consider
352 the predicted variations in ice cover.

353 *The poles:* Due to its low elevation, the present-day North Pole is not among the
354 strongest cold traps in early Mars climate simulations except at relatively low surface
355 pressure or very low spin-axis obliquity (e.g. Wordsworth et al., 2015). However, as
356 discussed above, there is widespread agreement between GCMs that the South Pole is a
357 highly favorable location for ice accumulation at higher-than-present surface pressure and
358 low to moderate spin-axis obliquity. The early Hesperian-aged Dorsa Argentea Formation
359 (DAF; Figure 5), with two lobes extending up to 30 degrees of latitude northward from the
360 south pole of Mars along the 0°W and 90°W meridians, has long been interpreted as the
361 remnants of a large former ice sheet (Allen, 1979, Howard, 1981, Kargel and Strom, 1992,
362 Head and Pratt, 2001). While the asymmetric shape of the DAF had previously been

363 attributed to differential erosion (Head and Pratt, 2001, Kite et al., 2009), GCM and ice
 364 flow model simulations indicate that an extensive south polar ice sheet would have this
 365 footprint as a natural consequence of regional topography in a thicker atmosphere (Scanlon
 366 et al., 2018). The flat-topped, steep-sided Sisyphi Montes are interpreted as englacial
 367 volcanoes recording a minimum ice thickness of 1400 meters at the time of eruption
 368 (Ghatan and Head, 2002). This hypothesis is further supported by spectroscopic evidence
 369 for hydrothermal alteration (Ackiss and Wray, 2014, Ackiss et al., 2018). The “Dorsa
 370 Argentea” ridges for which the formation is named (Head and Pratt, 2001, Kress and Head,
 371 2015, Butcher et al., 2016, Scanlon et al., 2018), steep-walled pits or “cavi” in the plains
 372 of the DAF (Ghatan et al., 2003, Dickson and Head, 2006), and outflow channels (Ghatan
 373 and Head, 2004) and breached basins (Milkovich et al., 2002, Dickson and Head, 2006) at
 374 the margins of the DAF are interpreted as glaciofluvial features that together record
 375 widespread melting of the ice sheet.



377

378 **Figure 5:** A. The Dorsa Argentea Formation, with units as mapped by Tanaka et al. (2014)
379 and hypothesized glacial, glaciovolcanic, and glaciofluvial features as mapped by Scanlon
380 et al. (2018). B. The flat-topped, steep-sided Sisyphi Montes are interpreted as subglacial
381 volcanoes, or tuyas (Ghatan and Head, 2004); MOLA altitude shading (Smith et al., 2003)
382 on THEMIS daytime IR 100 m global basemap (Edwards et al., 2011). C. The Cavi Angusti
383 are interpreted as glacial melt features (Ghatan et al., 2003); MOLA altitude shading on
384 THEMIS daytime IR 100 m global basemap.

385

386 The hypothesis that the Dorsa Argentea ridges are eskers, i.e. the depositional
387 remnants of subglacial channels (Figure 3, upper panels; e.g. Cuffey and Paterson, 2010),
388 is particularly well-supported: the distribution of length and sinuosity among the ridges are
389 statistically similar to those of Canadian eskers formed beneath the Laurentide Ice Sheet
390 (Figure 3, upper right panel; Butcher et al., 2016, Storrar et al., 2013, 2014, 2015), and the
391 relationship of ridge height to underlying topography is as expected if the ridges were
392 deposited in pressurized subglacial channels (Head and Hallet, 2001, Butcher et al., 2016).

393

394 The LMD GCM and University of Maine Ice Sheet Model (UMISM) only predict
395 a large south polar ice sheet with 0° and 90°W lobes like those of the DAF when the Tharsis
396 bulge is present and the poles are in their present location (Scanlon et al., 2018), and the
397 crater ages for the exposure of the Dorsa Argentea eskers (3.83 – 3.41 Ga; Kress and Head,
398 2015) and the cessation of activity in the equatorial valley networks (3.81 – 3.45 Ga; Fassett
399 and Head, 2008a) closely overlap. This is difficult to reconcile with the hypothesis (Bouley
400 et al., 2016) that the valley networks formed before the Tharsis bulge. If the valley networks
401 predate Tharsis but the south circumpolar ice sheet only has the shape and location of the
402 DAF if Tharsis is in place, the DAF eskers should be younger than the valley networks,
403 and their exposure ages younger still. Given the inherent uncertainties in crater dating, one
404 could speculate that valley network cessation might predate the removal of the ice
overlying the DAF eskers despite the similar ages from crater counts (i.e. that valley

405 network cessation, true polar wander, and the construction and retreat of the DAF all
406 occurred within a shorter time span than the margin of uncertainty in the crater ages), or
407 that valley network activity might have continued in the “rain shadow” east of Tharsis after
408 the completion of true polar wander due to low-obliquity excursions or the melting of ice
409 that had been emplaced before true polar wander. Alternatively, true polar wander may not
410 be necessary to explain the distribution of valley networks (cf. Guzewich et al., 2021).

411 For reasonable estimates of the total Noachian/Hesperian water inventory, some
412 degree of warming above the CO₂/H₂O baseline was likely required for basal melting of a
413 south polar ice sheet (Scanlon et al., 2018). Along with the strong likelihood of Tharsis
414 glaciation in any warm climate, this underscores that even if the climate of early Mars was
415 warm enough for rainfall in some regions, glacial processes would still have played an
416 important role in others. It is increasingly clear (Wordsworth et al., 2018, Kamada et al.,
417 2020, Guzewich et al., 2021, Schmidt et al., 2022) that both the “warm and wet” and “cold
418 and icy” endmembers are tools for understanding the complex whole of ancient Mars
419 paleoclimate rather than complete pictures in themselves.

420 **III. Question 2: What fraction of observed fluvial geology on Mars is due to ice melt?**

421 Thousands of valley networks incise the southern Martian highlands, speaking of a
422 past with surface water activity. Whereas the community has largely interpreted these
423 drainage systems in terms of a ‘warm and wet’ environment, the possibility that a more or
424 less significant fraction of these valleys formed through glaciofluvial processes related to
425 an ‘Icy Highlands’ ice sheet has been increasingly considered (Fastook and Head, 2015,
426 Cassanelli and Head, 2019, Bouquety et al., 2019 and 2020, Grau Galofre et al., 2020a). In
427 this scenario, the formation of valley networks involves sporadic or continued production

428 of meltwater, encompassing different degrees of ice cover that include melting of
429 snowpacks, ice marginal streams sourced from supraglacial meltwater, and subglacial
430 streams. This hypothesis is supported by statistical analyses of valley network
431 morphometry, by erosion rates of analogue snow and ice melt valleys in Antarctica, and by
432 the presence of morphological characteristics (constant width downstream, longitudinal
433 profile undulations, discontinuous valley segments, etc) that are consistent with subglacial,
434 but not fluvial, erosion (Lee et al., 1999, Fastook and Head, 2015, Cassanelli and Head,
435 2019, Grau Galofre et al., 2020a).

436 In the ‘warm and wet’ hypothesis, the origin of the martian valleys is generally
437 attributed to rainfall and surface runoff, which may or may not involve contributions from
438 groundwater seepage (Malin and Carr, 1999, Gulick, 2001, Craddock and Howard, 2002,
439 Howard et al., 2005, Hynek et al., 2010, Lamb et al., 2006, Irwin et al., 2011). Support for
440 this hypothesis comes from the similarity in planform morphology to possible analogue
441 rivers on Earth, as well as morphometrical quantities such as drainage density, network
442 topology, and relationship with drainage divides (e.g., Craddock and Howard, 2002, Hynek
443 et al., 2010). This environmental endmember often contemplates the existence of a northern
444 ocean, which would have occupied the northern lowlands extending north from the
445 dichotomy boundary, along two proposed shorelines: Deuteronilus and Arabia. This
446 hypothesis is consistent with the distribution of deltas, the elevation of the equipotential
447 curve, and possible tsunami deposits (Baker et al., 1991, Perron et al., 2007, Di Achille and
448 Hynek, 2010, Rodriguez et al., 2016, Costard et al., 2017, Costard et al., 2019, De Blasio,
449 2020). However, rainfall and/or melt of snowpacks fail to explain aspects of valley network

450 morphology, in particular the lack of dissection between consecutive drainage basins, and
451 the invariant widths along the valleys (Grau Galofre et al., 2020a).

452 Grau Galofre et al. (2020a) studied the origin of a subset of the global database of
453 valley networks and classified them by their most likely origin based on statistical
454 morphometry. The study found that, whereas rivers and sapping valleys explain a large
455 percentage of valley network morphologies, a fraction of them is most consistent with
456 channels formed under ancient ice sheets, akin to the Finger Lakes in New York, or the
457 subglacial channel networks found on Devon Island (Canadian Arctic Archipelago, Lee et
458 al., 1999, Grau Galofre et al., 2020a). Morphological similarities between valley networks
459 and subglacial channels, noted also regionally in Bouquety et al.(2019 and 2020), as well
460 as the spatial correlation of valley network locations with the near-marginal regions of a
461 proposed late Noachian icy highlands ice sheet provide support for the existence of such
462 an ice sheet with presence of localized basal melt (Fastook and Head, 2015, Bouquety et
463 al., 2019 and 2020, Grau Galofre et al., 2020a). Whereas the exact origin of the Martian
464 valley networks is still disputed, there is a general consensus that they were not active for
465 a long period of time, and that they did not achieve a large degree of landscape modification
466 (Fassett and Head, 2008a, Som et al., 2009, Penido et al., 2013, Grau Galofre et al., 2020b).

467 Fretted terrain, located in the transitional zone between the southern highlands and
468 the northern lowlands, and in particular Aeolis Mensae and Deuteronilus-Protonilus
469 Mensae (133°-147°E and 15°-55°E), display enigmatic terrains consisting of mesas of
470 complex planimetric configuration and sinuous valleys (Parker et al., 1989, Carr, 2001,
471 Head et al., 2006a). Whereas the exact origin of this terrain is under debate, some
472 hypotheses have brought forward the idea of Hesperian aged wet-based glaciation. In

473 particular, fretted valleys such as Mamers, Auqakuh, or Clasia Vallis, display
474 characteristics typical of integrated valley glacial systems on Earth, including multiple
475 theater-headed, alcove-like accumulation areas, U-shaped or box-shaped cross-sections,
476 sharp arete-like ridges (see glacial valleys and analogues shown in Figure 3, bottom
477 panels), converging patterns of downslope valley flow, valley lineation patterns typical of
478 ice deformation, streamlines indicative of flow around obstacles, and broad piedmont-like
479 lobes in the valley termination (Head et al., 2006a and b). Whereas some of these
480 characteristics, such as present-day valley infill and lineated patterns, are Amazonian in
481 age, erosion by wet-based glaciation is required to sculpt cirques, aretes, and U-shaped
482 valleys (e.g., Eyles, 1983, Benn et al., 2003, Harbor et al., 1988, Brook et al., 2006, Davila
483 et al., 2013). Substantial ice covers, ranging from 1000-2500 m thick, and dated from the
484 Late Noachian to the Early Hesperian, have been suggested to explain the morphology,
485 high flow lines, orientation, and extent of the fretted valleys (Davila et al., 2013, Dickson
486 et al., 2008, Morgan et al., 2009).

487 A key missing piece of geological evidence for a late Noachian icy highlands ice sheet
488 is the existence of scouring marks and lineated features, such as drumlins, mega-scale
489 glacial lineations, or ribbed moraines, which map the direction of glacial sliding, and which
490 are common indicators of the extent of terrestrial Quaternary ice sheets (e.g., Svendsen et
491 al., 2004, Fowler, 2014, Fastook and Head, 2015, Wordsworth, 2016, Ramirez and
492 Craddock, 2018, Gallagher et al., this volume).

493 Three explanations for this lack of features have been proposed. First, the late
494 Noachian icy highlands ice sheet did not exist (Ramirez and Craddock, 2018), requiring an
495 unknown greenhouse gas that would maintain surface temperatures above freezing and

496 inhibit the nucleation of significant portions of surface snow, preventing the ice-albedo
497 feedback. Second, a late Noachian icy highlands ice sheet existed but was fundamentally
498 cold-based, preventing glacial sliding except in very localized areas, and thus the
499 development of any characteristic lineated landform and the areal scouring of the substrate
500 (Fastook and Head, 2015, Wordsworth, 2016). This scenario hints at surface temperatures
501 at or below freezing, an ice cover up to 2 km thick, and a water inventory under 5X present
502 GEL (Global Equivalent Layer). The third possibility involves the role of surface gravity
503 in setting the dominant mode of glacial drainage. Even if water accumulated under a late
504 Noachian icy highlands ice sheet, the development of high efficiency drainage channels
505 under ice could prevent significant glacial sliding from developing on Mars in comparison
506 to Earth, producing a geological record that would differ from that characteristic of
507 Quaternary glaciation (Grau Galofre et al., 2022). The third hypothesis is also consistent
508 with the lack of sliding recorded in the DAF.

509 **IV. Question 3: How did the subsurface water inventory and cryosphere evolve with**
510 **time, and what is its effect on the global hydrologic cycle?**

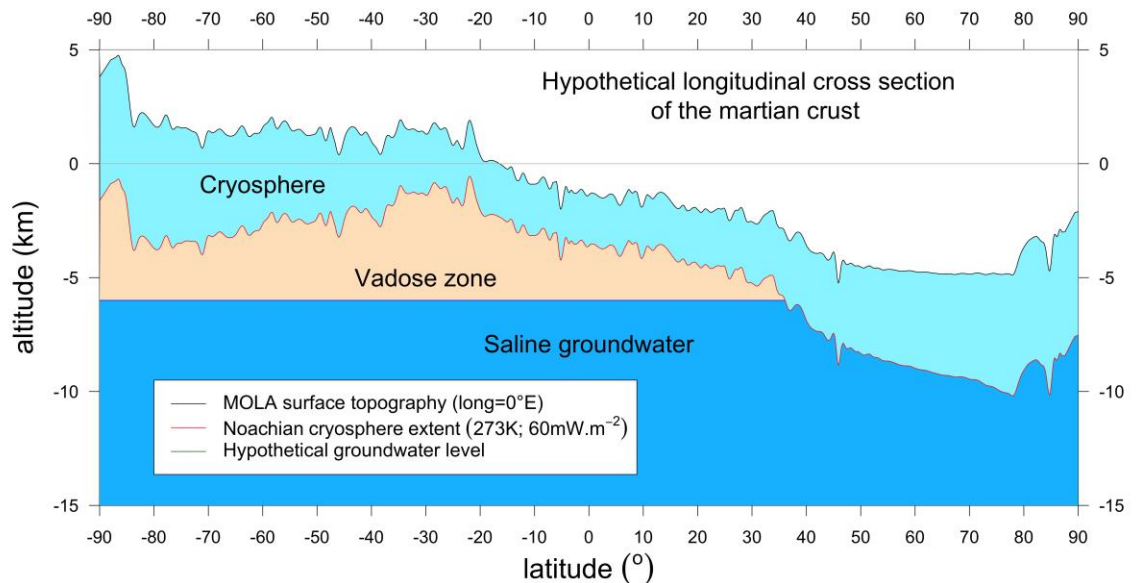
511 *Onset of a Noachian cryosphere and its impact on the hydrologic cycle.* As
512 discussed in the previous sections, strong evidence points to the fact that liquid water must
513 have been more abundant on Mars' surface during the Noachian than at any time since.
514 Therefore, the early Mars hydrology may have been similar to relatively arid environments
515 on present-day Earth, where precipitation, surface runoff and infiltration led to the
516 existence of standing bodies of water, lakes and possibly oceans (e.g. Palumbo and Head
517 2019, Guzewich et al., 2021, Schmidt et al., 2022), and an associated underlying
518 groundwater system (Clifford, 1993, Clifford and Parker, 2001). While early Mars may

519 have been warm and wet, the less degraded nature of post-Noachian terrains suggests a
520 geologically rapid transition to less erosive conditions, similar to those that exist on Mars
521 today (Carr, 1999, Kreslavsky and Head, 2018). As the planet transitioned to a colder
522 climate, a freezing front developed from the planet's surface through its crust, creating a
523 growing cold-trap for both atmospheric and subsurface H₂O—a region known as the
524 cryosphere as illustrated in Figure 6. The downward propagation of this freezing front, in
525 response to the planet's long-term decline in geothermal heat flux, had two important
526 consequences for the nature of the planet's hydrologic cycle and the state and distribution
527 of subsurface water.

528 First, ice condensed in the pores of the near-surface regolith would seal away any
529 groundwater from the atmosphere. This would result in a ground-ice depth distribution
530 primarily governed by the thermal structure of the crust, in effect mirroring to the first order
531 the local surface topography as illustrated in Figure 6. Taking into account reasonable
532 values of crustal permeability (i.e., column averaged values of $\sim 10^{-15}$ m² within the top
533 10 km, Clifford, 1993, Manning and Ingebritsen, 1999, Clifford and Parker, 2001), the
534 elimination of atmospheric recharge would rapidly lead to the decay of any precipitation-
535 driven influence on the shape of the global water table in 10^6 to 10^8 years. In the absence
536 of major seismic or thermal disturbances of the crust (such as those caused by large
537 impacts, earthquakes and volcanic activity), the liquid water at depth would have
538 constituted an aquifer in hydrostatic equilibrium, saturating the lowermost porous regions
539 of the crust. Due to the large range in surface altimetry on Mars (Aharonson et al., 2001),
540 the vertical distance between the base of the cryosphere and the groundwater table may
541 have varied considerably, creating an intervening unsaturated zone (also called vadose

542 zone), whose thickness was maximized in regions of high elevation and minimized (or
 543 absent) at low elevation.

544 Second, as the cryosphere extent deepened with time (by decreasing geothermal
 545 flux and surface equilibrium temperatures), the condensation of ice behind the advancing
 546 freezing-front would have created a growing sink for the planet's inventory of
 547 groundwater. Where the cryosphere and water table were in direct contact, the groundwater
 548 would have frozen to the base of the cryosphere as the freezing front propagated downward
 549 with time. However, in many locations throughout the highlands, the vertical distances
 550 separating the base of the cryosphere from the water table may have been several
 551 kilometers or more. Under such conditions, the depletion of groundwater is expected to
 552 have occurred via the thermally induced diffusion of vapor from warmer depths to the
 553 colder pores under the advancing freezing-front (Clifford, 1991 and 1993, Clifford and
 554 Parker, 2001).



555

556 **Figure 6:** Hypothetical meridian cross section of the Noachian Martian crust (along 0°E,
 557 a longitude representative of the global North-South dichotomy). The figure illustrates the

558 potential relationship between surface topography, ground ice and groundwater. The
559 vadose zone is a potential subsurface zone where saline groundwater exchanges with the
560 bottom part of the cryosphere by unsaturated vapor circulation. The lower level of the
561 cryosphere is calculated from the subsurface heat propagation model with a geothermal
562 flux of 60 mW m^{-2} and a 273K melting point of water (Surface topography from MOLA;
563 (Smith et al., 2001); cryosphere depth from (Schwenzer et al., 2012); Figure adapted from
564 (Clifford, 1993).

565
566 *Potential extent of the Late Noachian cryosphere.* We use a one-dimensional finite
567 difference thermal model of the subsurface (Clifford et al., 2010, Schwenzer et al., 2012)
568 to calculate Martian mean annual surface temperatures and the insolation heat wave
569 propagation through the Late Noachian cryosphere. The calculations assume that: (1) the
570 thermal conductivity of ice-saturated basalt varies with temperature following a simple
571 inverse law (Clifford et al., 2010; Hobbs, 1974); (2) the mean value of Late Noachian
572 geothermal heat flux can be deduced from estimates of the rheologic properties of the
573 Martian lithosphere necessary to support the relief of the Noachian topography (McGovern
574 et al., 2002 and 2004, Grott et al., 2005); (3) the Martian atmosphere at that time did not
575 induce a significant greenhouse effect as compared to current surface conditions and (4)
576 the variations in Martian obliquity and orbital eccentricity were comparable to those of
577 today. This last assumption's validity is largely dependent on the early developmental state
578 of Tharsis at that time which would have led to true polar wander of the orientation of the
579 planet. A late growth of Tharsis would lead to significant shifts in the position of the deep
580 cryosphere border, while not influencing majorly the overall results regarding the global
581 cryosphere extent and trapped water inventory (Bouley et al., 2016, Ward et al., 1979).

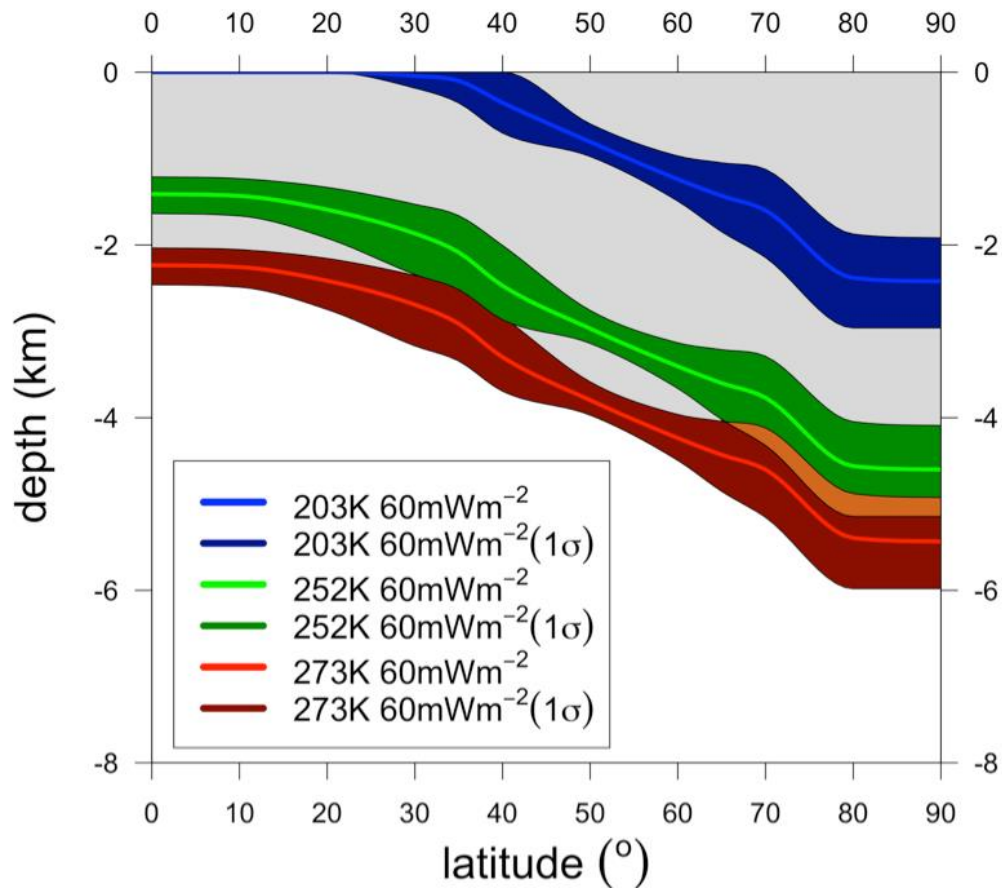
582 Figure 7 illustrates the variation in the depth of the cryosphere as a function of
583 latitude based on the average and extreme obliquity and orbital eccentricity values of
584 Laskar et al., (2004), combined with an assumed Noachian geothermal heat flux of

585 60 mW m⁻² (McGovern et al., 2004, Grott et al., 2005) and three groundwater freezing
586 temperatures depending on its salt content. The brine models considered correspond to pure
587 water (273 K) and eutectic brines of NaCl (252 K) and of Mg(ClO₄)₂ (203 K). One expects
588 salty brines as groundwater on Mars from the combination of crustal rock leaching over
589 hundreds of million years, vadose zone hydrothermal circulation of liquid water and the
590 reduction of groundwater volume in response to the cryosphere growth with time (Clifford
591 et al., 2010). In situ observations have shown that martian soil could contain up to 25wt.%
592 of salts (Clark and Van Hart, 1981). The study of salt abundances in fractures of Nakhlite
593 meteorites have also indicated the evaporative salt deposition from concentrated brines as
594 well as dilute brines giving constraints on the fluid salt concentration on Mars (Rao et al.,
595 2005 and 2008, Bridges and Schwenzer, 2012). NaCl has been detected on Mars and is
596 expected to be a common salt, with a eutectic freezing temperature of 252K. This
597 corresponds to the first brine considered in our model.

598 Chloride and sulfur rich salts are also expected with varying freezing depression
599 points typically lower than the one for NaCl brines, for example it is 238K for a eutectic
600 solution of MgCl₂ and 218K for a eutectic solution of CaCl₂ (Burt and Knauth, 2003, Fairén
601 et al., 2009). However, the concentrations of the different salt species in martian
602 underground water are not well constrained. The detection of perchlorate in the regolith of
603 Mars (Hecht et al., 2009, Clark et al., 2021) and its ability to be readily dissolved suggest
604 it may have infiltrated in the underground water system of Mars (Clifford et al., 2010). The
605 strong freezing depression point of perchlorates (as low as 203K for Mg(ClO₄)₂) is used as
606 our second brine model for the cryosphere, as an extreme case to determine the limits of
607 validity of the cryosphere extent. While it is unlikely that brines fully saturated in

608 magnesium perchlorate salts exist globally on the planet (Hecht et al., 2009, Glavin et al.,
 609 2013, Kounaves et al., 2014), the simulations using such a low freezing depression point
 610 give a lower limit to the depth of the cryosphere that can be reached by groundwater brines
 611 with mixed salts located in the underground.

612 .



613

614 **Figure 7:** Depth of the Martian cryosphere as a function of latitude assuming a Noachian
 615 geothermal heat flux of 60mW m^{-2} . The three colored lines correspond to the average
 616 cryosphere depth for different brine salt contents: pure water (273K); NaCl brine (252K)
 617 and perchlorate brine (203K). The colored area around the average depth corresponds to
 618 statistical variations due to the orbital parameters of Mars with time (Laskar et al., 2004,
 619 Schwitzer et al., 2012)

620

621 The calculated equilibrium depths of a pure water cryosphere are represented in
622 Figure 6. The cryosphere maximum depth ranges from 2.3 km at the equator to 5.6 km near
623 the poles (assuming a pure water depression freezing point of 273 K). This latitudinal
624 variation is due to the colder average annual temperatures near the poles resulting from
625 both a lower insolation and the higher albedo of the seasonal and perennial polar ice
626 deposits, compared to Mars' typical regolith. The polar deposits are assumed to be similar
627 in extent to today's polar caps. The depth of the cryosphere would be much reduced under
628 the conditions relevant for brines. For example, in the case of a solution saturated in
629 magnesium perchlorate (i.e., 203 K), the cryosphere extent would reach its maximum of
630 2.5 km around the poles and continuously decrease with lower latitudes until it completely
631 disappears at latitudes of less than about 30-35°, where mean annual temperatures exceed
632 the assumed perchlorate-depressed freezing point of groundwater.

633 On Figure 7, the colored thickness of the lines corresponds to simulations of the
634 high and low extreme 1σ Mars orbital parameters (obliquity and eccentricity) assuming a
635 20 Ma obliquity history equivalent to the nominal current model of Laskar et al. (2004).
636 Such variations in orbital parameters translate into a 0.5 km depth change at the equator
637 and a 1 km depth change at the poles, these two changes compensating on average one
638 another due to the change in obliquity of the planet.

639 *Water content in the Noachian cryosphere.* Once established and stabilized, the
640 global planet cryosphere would act as an underground cold-trap in the pore volume of the
641 Martian crust for the available water. Assuming a surface porosity of 0.2 and a typical
642 exponential depth decay constant of 2.82 km (Clifford, 1993, Clifford and Parker, 2001),
643 we can calculate the total pore volume available for this cold-trap over the entire planet at

644 the depth where the cryosphere reaches its maximum extent. The pure water Noachian
645 cryosphere model described in Figure 7 could have cold-trapped about 446 m (+/- 8 m)
646 GEL. As freezing-point depression salts are included, the depth of the cryosphere decreases
647 as well as the potential volume of water trapped. In the case of a NaCl saturated aquifer
648 (T=252K), the cryosphere could trap 390 m (+/- 15 m) GEL and for the more extreme
649 perchlorate saturated brine (T=203K), a volume corresponding to 104 m (+/- 13 m) GEL.
650 As we do not expect the aquifer water to be entirely saturated in salts, this is certainly
651 enough to trap a significant fraction or even the totality of the available liquid water
652 inventory expected at the end of the Noachian, as discussed in other studies (Carr and Head,
653 2015 and 2019, Palumbo and Head, 2020).

654 *Local variations in the cryosphere thickness and state.* The calculations presented
655 above correspond to the ideal case of a global cryosphere in equilibrium with the planet
656 surface and interior conditions. It is expected that local variations in geothermal heat flow,
657 and heat produced by volcanic activity as well as impacts, would locally temporarily affect
658 the extent of the cryosphere, or melt it entirely. Such heat events could generate specific
659 hydrothermal systems and have been suggested as a possible source for some of the fluvial
660 features detected on Mars (Gulick, 1998 and 2001). Even with a global cryosphere extent
661 as shown in Figure 7, it would have been thermally penetrated by relatively small
662 impactors, the heat generated by the impact being sufficient to melt the cryosphere over its
663 whole thickness. Calculations based on a model developed by Abramov and Kring (2005)
664 and applied to a two-layer Mars subsurface have shown that a 2-km thick cryosphere, like
665 around the equator, can be thermally penetrated by an impactor as small as 0.6 km in
666 diameter, while the thicker 6-km cryosphere below the poles would be thermally penetrated

667 by projectiles as small as 1.8 km in diameter (Schwenzer et al., 2012). Such impacts would
668 also occur more frequently during the Noachian era and lead to the generation of local
669 hydrothermal systems with liquid water lasting up to 10 million years due to the time
670 necessary for the dissipation of heat in the system (Schwenzer et al., 2012). This would
671 also further enable exchanges between the deep underground aquifers and the atmosphere.

672 Local changes in the depth of the cryosphere are expected due to local changes in
673 the geothermal heat flux of the planet. To this day, the average heat flux is around 25 mW
674 m⁻² but can still increase to 50 mW m⁻² in some locations (Plesa et al., 2016). Such high
675 heat flux may have resulted in geothermally induced melting at the base of the cryosphere
676 in the past. Such events can be linked with surficial meltwater features such as valley
677 networks and the location of hydrous minerals on Mars (Ojha et al., 2020). There is also
678 evidence that such processes have continued in the relatively recent past as candidate eskers
679 have been identified in Amazonian terrains, Phlegra Montes and Tempe Terra, for which
680 an origin from basal melting due to enhanced geothermal heat flux was suggested
681 (Gallagher and Balme, 2015, Butcher et al., 2017, Koutnik et al., 2023). Under such
682 conditions, it could even be envisioned that liquid water could accumulate as a northern
683 ocean fed by groundwater under sub-freezing Martian surface climate (Palumbo and Head,
684 2019). The existence of an ocean with a frozen surface would be consistent with the
685 relatively low level of erosion of Hesperian age terrains, but would be inconsistent with
686 reported geological evidence for tsunami emplacement (Costard et al., 2017, Rodriguez et
687 al., 2016, Costard et al., 2019).

688 As the cryosphere would continue to extend, and conditions for melting became
689 rarer, it is possible that the ice-cemented cryosphere (the part of the cryosphere where pores

690 are completed saturated by ice) would seal away liquid groundwater at depth that could
691 remain there to this day, without the possibility of escape (Grimm et al., 2017). However,
692 there has been no detected evidence of such a global reservoir of ice and liquid water at
693 depth to date, either from radars (Clifford et al., 2010) or from seismometry (Manga and
694 Wright, 2021). The morphology of the Hesperian-Amazonian-aged single-layered ejecta
695 crater indicate a smaller extent of cemented cryosphere at the Hesperian to Amazonian
696 transition, with an estimated maximum depth of 1.3 km at the equator and 2.3 km at the
697 poles (Weiss and Head, 2017). The volume considered corresponds to 200 m GEL
698 assuming ~20% porosity at the surface. Comparing it to the results given in Figure 7, it
699 would mean that the available pore volume that could be filled by ice was supply limited
700 in the cases of the pure water ice (446 m GEL), or saturated NaCl brine (390 m GEL)
701 cryospheres which never reached saturation. The single-layered ejecta crater observations
702 can be consistent with a perchlorate salts brine (104 m GEL) fully saturated cryosphere;
703 though this remains an extreme case of salt saturation that is certainly less likely. This
704 would mean that the majority of subsurface water inventory of Mars during the Hesperian,
705 up to 200 m GEL from the single-layered ejecta crater observations, would have been fully
706 trapped in the expected cryosphere volumes (Weiss and Head, 2017). As a consequence,
707 no underground extensive liquid water aquifers probably exist today on the planet while
708 about 30 m GEL of water still exists above the surface to form the currently visible polar
709 caps (Lasue et al., 2012, Carr and Head, 2015, Villanueva et al., 2015). This is also
710 consistent with the seismic velocity investigations made by the InSight mission on Mars,
711 indicating that there is no pore ice saturation of the upper 10 km of the Martian crust at
712 Elysium Planitia (Manga and Wright, 2021).

713 **V. Conclusions**

714 While the extent of surface ice on early Mars remains as uncertain as the rest of the
715 climate, the use of three-dimensional GCMs to investigate possible climates continues to
716 generate hypotheses for geologists to test. The glacial geomorphological record
717 corresponding to early Mars is notoriously difficult to interpret, as many features that have
718 possible glacial interpretations are ambiguous, are heavily degraded, and/or are covered in
719 later deposits (e.g. the latitude-dependent mantle, LDM). In particular, even very large
720 cold-based Noachian or Hesperian ice sheets may never have left evidence capable of
721 surviving to the present day, save for possible effects on volcanic flows that encountered
722 them or on the impact cratering record. It is a worthwhile exercise to consider what any
723 given observed Amazonian glacial landform (Koutnik et al., 2023) might look like after 3
724 Ga of impact cratering, aeolian erosion, and subsequent glacial cycles. Still, case studies
725 of regional landform assemblages lend increasing support to the presence of Noachian and
726 Hesperian ice sheets in regions such as the Isidis basin and the high southern latitudes, and
727 global statistical studies of valley morphometry and impact crater degradation are a
728 promising avenue for greater clarity on the prevalence of ice across space and time.
729 Furthermore, recent work has highlighted the discrepancies that should be expected
730 between terrestrial and Martian glacial landscapes, warranting a fresh examination of
731 Martian glacial geology, both ancient and modern.

732 During the Noachian to Hesperian transition, it is expected that the decreasing
733 geothermal heat flux and global surface temperatures induced the onset of a global
734 subsurface cryosphere formation, which would have cold-trapped subsurface Martian
735 water in the crustal pore system. The extant surface water ice of modern Mars, having

736 decreased in abundance throughout the Hesperian and into the Amazonian by this and other
 737 mechanisms, provides another window to how water ice interacts with volcanic,
 738 atmospheric, impact and aeolian processes to affect the Martian geologic record (Koutnik
 739 et al., 2023).

740 **Acknowledgements**

741 The authors would like to kindly thank the time and effort of the three reviewers that
 742 considered this manuscript, whose queries led to significant improvements, as well as
 743 insightful discussions with F. Butcher and comments by J.P. Williams. AGG
 744 acknowledges the funding received from the European Union's Horizon 2020 research
 745 and innovation program under the Marie Skłodowska-Curie grant agreement MGFR
 746 101027900, and from the School of Earth and Space Exploration (ASU) through the
 747 Exploration Fellowship. KES gratefully acknowledges support from the NASA
 748 Postdoctoral Program at Goddard Space Flight Center, administered by ORAU under
 749 contract with NASA.

750

751 **References**

752

- 753 Abramov, O., & Kring, D. A. (2005). Impact-induced hydrothermal activity on early
 754 Mars. *Journal of Geophysical Research: Planets*, *110*(E12).
- 755 Ackiss, S., Horgan, B., Seelos, F., Farrand, W., & Wray, J. (2018). Mineralogic evidence
 756 for subglacial volcanism in the Sisyphi Montes region of Mars. *Icarus*, *311*, 357-370
- 757 Ackiss, S. E., & Wray, J. J. (2014). Occurrences of possible hydrated sulfates in the
 758 southern high latitudes of Mars. *Icarus*, *243*, 311-324.
- 759 Aharonson, O., Zuber, M. T., & Rothman, D. H. (2001). Statistics of Mars' topography
 760 from the Mars Orbiter Laser Altimeter: Slopes, correlations, and physical
 761 models. *Journal of Geophysical Research: Planets*, *106*(E10), 23723-23735.
- 762 Allen, C. C. (1979). Volcano-ice interactions on Mars. *Journal of Geophysical Research:*
 763 *Solid Earth*, *84*(B14), 8048-8059.
- 764 Archer, B. R., Hynek, B. M., & Robbins, S. J. (2021, March). Crater Evidence Does Not
 765 Support the Late Noachian Icy Highlands for Mars. In *52nd Lunar and Planetary*
 766 *Science Conference* (No. 2548, p. 2220).
- 767 Baker, V. R. (2001). Water and the Martian landscape. *Nature*, *412*(6843), 228-236.
- 768 Baker, V. R., Strom, R. G., Gulick, V. C., Kargel, J. S., Komatsu, G., & Kale, V. S.
 769 (1991). Ancient oceans, ice sheets and the hydrological cycle on
 770 Mars. *Nature*, *352*(6336), 589-594.
- 771 Balco, G. (2011). Contributions and unrealized potential contributions of cosmogenic-
 772 nuclide exposure dating to glacier chronology, 1990–2010. *Quaternary Science*
 773 *Reviews*, *30*(1-2), 3-27.
- 774 Banks, M. E., Lang, N. P., Kargel, J. S., McEwen, A. S., Baker, V. R., Grant, J. A., ... &
 775 Strom, R. G. (2009). An analysis of sinuous ridges in the southern Argyre

- 776 Planitia, Mars using HiRISE and CTX images and MOLA data. *Journal of*
 777 *Geophysical Research: Planets*, 114(E9).
- 778 Batalha, N. E., Koppalapu, R. K., Haqq-Misra, J., & Kasting, J. F. (2016). Climate
 779 cycling on early Mars caused by the carbonate–silicate cycle. *Earth and Planetary*
 780 *Science Letters*, 455, 7-13.
- 781 Benn, D. I., Kirkbride, M. P., Owen, L. A., & Brazier, V. (2003). Glaciated valley
 782 landsystems. *Glacial landsystems*, 372-406.
- 783 Bernhardt, H., Reiss, D., Hiesinger, H., & Ivanov, M. A. (2016). The honeycomb terrain
 784 on the Hellas basin floor, Mars: A case for salt or ice diapirism. *Journal of*
 785 *Geophysical Research: Planets*, 121(4), 714-738.
- 786 Bernhardt, H., Reiss, D., Ivanov, M., Hauber, E., Hiesinger, H., Clark, J. D., & Orosei, R.
 787 O. B. E. R. T. O. (2019). The banded terrain on northwestern Hellas Planitia: New
 788 observations and insights into its possible formation. *Icarus*, 321, 171-188.
- 789 Bernhardt, H., Hiesinger, H., Reiss, D., Ivanov, M., & Erkeling, G. (2013). Putative
 790 eskers and new insights into glacio-fluvial depositional settings in southern
 791 Argyre Planitia, Mars. *Planetary and Space Science*, 85, 261-278.
- 792 Black, B. A., Perron, J. T., Hemingway, D., Bailey, E., Nimmo, F., & Zebker, H. (2017).
 793 Global drainage patterns and the origins of topographic relief on Earth, Mars, and
 794 Titan. *Science*, 356(6339), 727-731.
- 795 Boatwright, B. D., & Head, J. W. (2021). A Noachian proglacial paleolake on Mars:
 796 fluvial activity and lake formation within a closed-source drainage basin crater
 797 and implications for early Mars climate. *The Planetary Science Journal*, 2(2), 52.
- 798 Bouley, S., Baratoux, D., Matsuyama, I., Forget, F., Séjourné, A., Turbet, M., & Costard,
 799 F. (2016). Late Tharsis formation and implications for early
 800 Mars. *Nature*, 531(7594), 344-347.
- 801 Bouquety, A., Sejourné, A., Costard, F., Mercier, D., & Bouley, S. (2019). Morphometric
 802 evidence of 3.6 Ga glacial valleys and glacial cirques in martian highlands: South
 803 of Terra Sabaea. *Geomorphology*, 334, 91-111.
- 804 Bouquety, A., Sejourné, A., Costard, F., Bouley, S., & Leyguarda, E. (2020). Glacial
 805 landscape and paleoglaciation in Terra Sabaea: Evidence for a 3.6 Ga polythermal
 806 plateau ice cap. *Geomorphology*, 350, 106858.
- 807 Bridges, J. C., & Schwenzer, S. P. (2012). The nakhlite hydrothermal brine on
 808 Mars. *Earth and Planetary Science Letters*, 359, 117-123.
- 809 Bristow, T. F., Haberle, R. M., Blake, D. F., Des Marais, D. J., Eigenbrode, J. L., Fairén,
 810 A. G., ... & Vasavada, A. R. (2017). Low Hesperian P CO₂ constrained from in
 811 situ mineralogical analysis at Gale Crater, Mars. *Proceedings of the National*
 812 *Academy of Sciences*, 114(9), 2166-2170.
- 813 Brook, M. S., Kirkbride, M. P., & Brock, B. W. (2006). Cirque development in a steadily
 814 uplifting range: rates of erosion and long-term morphometric change in alpine
 815 cirques in the Ben Ohau Range, New Zealand. *Earth Surface Processes and*
 816 *Landforms: The Journal of the British Geomorphological Research Group*, 31(9),
 817 1167-1175.
- 818 Burt, D. M., & Knauth, L. P. (2003). Electrically conducting, Ca-rich brines, rather than
 819 water, expected in the Martian subsurface. *Journal of Geophysical Research:*
 820 *Planets*, 108(E4).

- 821 Butcher, F. E., Conway, S. J., & Arnold, N. S. (2016). Are the dorsa argentea on mars
822 eskers?. *Icarus*, 275, 65-84.
- 823 Butcher, F. E., Balme, M. R., Gallagher, C., Arnold, N. S., Conway, S. J., Hagermann,
824 A., & Lewis, S. R. (2017). Recent basal melting of a mid-latitude glacier on
825 Mars. *Journal of Geophysical Research: Planets*, 122(12), 2445-2468.
- 826 Cabrol, N. A., & Grin, E. A. (1999). Distribution, classification, and ages of Martian
827 impact crater lakes. *Icarus*, 142(1), 160-172.
- 828 Carr, M. H., & Head, J. W. (2015). Martian surface/near-surface water inventory:
829 Sources, sinks, and changes with time. *Geophysical Research Letters*, 42(3), 726-
830 732.
- 831 Carr, M., & Head, J. (2019). Mars: Formation and fate of a frozen Hesperian
832 ocean. *Icarus*, 319, 433-443.
- 833 Carr, M. H. (1995). The Martian drainage system and the origin of valley networks and
834 fretted channels. *Journal of Geophysical Research: Planets*, 100(E4), 7479-7507.
- 835 Carr, M. H. (2001). Mars Global Surveyor observations of Martian fretted
836 terrain. *Journal of Geophysical Research: Planets*, 106(E10), 23571-23593.
- 837 Carr, M. H. (1999). Retention of an atmosphere on early Mars. *Journal of Geophysical
838 Research: Planets*, 104(E9), 21897-21909.
- 839 Carr, M. H. (2007). *The surface of Mars* (Vol. 6). Cambridge University Press.
- 840 Cassanelli, J. P., & Head, J. W. (2019). Glaciovolcanism in the Tharsis volcanic province
841 of Mars: Implications for regional geology and hydrology. *Planetary and Space
842 Science*, 169, 45-69.
- 843 Cassanelli, J. P., Head, J. W., & Fastook, J. L. (2015). Sources of water for the outflow
844 channels on Mars: Implications of the Late Noachian “icy highlands” model for
845 melting and groundwater recharge on the Tharsis rise. *Planetary and Space
846 Science*, 108, 54-65.
- 847 Cassata, W. S., Zahnle, K. J., Samperton, K. M., Stephenson, P. C., & Wimpenny, J.
848 (2022). Xenon isotope constraints on ancient Martian atmospheric escape. *Earth
849 and Planetary Science Letters*, 580, 117349.
- 850 Chapman, M. G., Neukum, G., Dumke, A., Michael, G., Van Gasselt, S., Kneissl, T., ...
851 & Mangold, N. (2010). Amazonian geologic history of the Echus Chasma and
852 Kasei Valles system on Mars: New data and interpretations. *Earth and Planetary
853 Science Letters*, 294(3-4), 238-255.
- 854 Chapman, M. G., Neukum, G., Dumke, A., Michael, G., Van Gasselt, S., Kneissl, T., ...
855 & Masson, P. (2010). Noachian–Hesperian geologic history of the Echus Chasma
856 and Kasei Valles system on Mars: New data and interpretations. *Earth and
857 Planetary Science Letters*, 294(3-4), 256-271.
- 858 Citron, R. I., Manga, M., & Tan, E. (2018). A hybrid origin of the Martian crustal
859 dichotomy: Degree-1 convection antipodal to a giant impact. *Earth and Planetary
860 Science Letters*, 491, 58-66.
- 861 Clark, B. C., & Van Hart, D. C. (1981). The salts of Mars. *Icarus*, 45(2), 370-378.
- 862 Clark, J., Sutter, B., Archer Jr, P. D., Ming, D., Rampe, E., McAdam, A., ... & Mahaffy,
863 P. (2021). A review of sample analysis at Mars-Evolved Gas Analysis Laboratory
864 analog work supporting the presence of perchlorates and chlorates in Gale Crater,
865 Mars. *Minerals*, 11(5), 475.

- 866 Clifford, S. M. (1991). The role of thermal vapor diffusion in the subsurface hydrologic
867 evolution of Mars. *Geophysical Research Letters*, 18(11), 2055-2058.
- 868 Clifford, S. M. (1993). A model for the hydrologic and climatic behavior of water on
869 Mars. *Journal of Geophysical Research: Planets*, 98(E6), 10973-11016.
- 870 Clifford, S. M., & Parker, T. J. (2001). The evolution of the Martian hydrosphere:
871 Implications for the fate of a primordial ocean and the current state of the northern
872 plains. *Icarus*, 154(1), 40-79.
- 873 Clifford, S. M., Lasue, J., Heggy, E., Boisson, J., McGovern, P., & Max, M. D. (2010).
874 Depth of the Martian cryosphere: Revised estimates and implications for the
875 existence and detection of subpermafrost groundwater. *Journal of Geophysical
876 Research: Planets*, 115(E7).
- 877 Costard, F., Séjourné, A., Kelfoun, K., Clifford, S., Lavigne, F., Di Pietro, I., & Bouley,
878 S. (2017). Modeling tsunami propagation and the emplacement of thumbprint
879 terrain in an early Mars ocean. *Journal of Geophysical Research: Planets*, 122(3),
880 633-649.
- 881 Costard, F., Séjourné, A., Lagain, A., Ormö, J., Rodriguez, J. A. P., Clifford, S., ... &
882 Lavigne, F. (2019). The Lomonosov crater impact event: A possible mega-
883 tsunami source on Mars. *Journal of Geophysical Research: Planets*, 124(7),
884 1840-1851.
- 885 Craddock, R. A., & Howard, A. D. (2002). The case for rainfall on a warm, wet early
886 Mars. *Journal of Geophysical Research: Planets*, 107(E11), 21-1.
- 887 Craddock, R. A., & Maxwell, T. A. (1993). Geomorphic evolution of the Martian
888 highlands through ancient fluvial processes. *Journal of Geophysical Research:
889 Planets*, 98(E2), 3453-3468.
- 890 Cuffey, K. M., & Paterson, W. S. B. (2010). *The physics of glaciers*. Academic Press.
- 891 Davila, A. F., Fairén, A. G., Stokes, C. R., Platz, T., Rodriguez, A. P., Lacelle, D., ... &
892 Pollard, W. (2013). Evidence for Hesperian glaciation along the Martian
893 dichotomy boundary. *Geology*, 41(7), 755-758.
- 894 De Blasio, F. V. (2020). Frontal Aureole Deposit on Acheron Fossae ridge as evidence
895 for landslide-generated tsunami on Mars. *Planetary and Space Science*, 187,
896 104911.
- 897 De Blasio, F. V. (2018). The pristine shape of Olympus Mons on Mars and the
898 subaqueous origin of its aureole deposits. *Icarus*, 302, 44-61.
- 899 Di Achille, G., & Hynek, B. M. (2010). Ancient ocean on Mars supported by global
900 distribution of deltas and valleys. *Nature Geoscience*, 3(7), 459-463.
- 901 Dickson, J. L., Head, J. W., & Marchant, D. R. (2008). Late Amazonian glaciation at the
902 dichotomy boundary on Mars: Evidence for glacial thickness maxima and
903 multiple glacial phases. *Geology*, 36(5), 411-414.
- 904 Dickson, J., & Head, J. W. (2006). Evidence for an Hesperian-aged south circum-polar
905 lake margin environment on Mars. *Planetary and Space Science*, 54(3), 251-272.
- 906 Dohm, J. M., Hare, T. M., Robbins, S. J., Williams, J. P., Soare, R. J., El-Maarry, M. R.,
907 ... & Maruyama, S. (2015). Geological and hydrological histories of the Argyre
908 province, Mars. *Icarus*, 253, 66-98.
- 909 Edwards, C. S., Nowicki, K. J., Christensen, P. R., Hill, J., Gorelick, N., & Murray, K.
910 (2011). Mosaicking of global planetary image datasets: 1. Techniques and data

- 911 processing for Thermal Emission Imaging System (THEMIS) multi-spectral
 912 data. *Journal of Geophysical Research: Planets*, 116(E10).
- 913 Erkeling, G., Reiss, D., Hiesinger, H., Ivanov, M. A., Hauber, E., & Bernhardt, H.
 914 (2014). Landscape formation at the Deuteronilus contact in southern Isidis
 915 Planitia, Mars: Implications for an Isidis Sea?. *Icarus*, 242, 329-351.
- 916 Eyles, N. (1983). Modern Icelandic glaciers as depositional models for «hummocky
 917 moraine» in the Scottish Highlands. In *INQUA Symposia on the genesis and*
 918 *lithology of quaternary deposits* (pp. 47-59).
- 919 Fairén, A. G., Davila, A. F., Gago-Duport, L., Amils, R., & McKay, C. P. (2009).
 920 Stability against freezing of aqueous solutions on early Mars. *Nature*, 459(7245),
 921 401-404.
- 922 Fan, B. M., Jansen, M. F., Mischna, M. A., & Kite, E. S. (2022). Why are Mountain-Tops
 923 Cold?—The Decorrelation of Surface Temperature and Topography Due to the
 924 Decline of the Greenhouse Effect on Early Mars. *LPI Contributions*, 2678, 1698.
- 925 Fassett, C. I., & Head III, J. W. (2008). The timing of martian valley network activity:
 926 Constraints from buffered crater counting. *Icarus*, 195(1), 61-89.
- 927 Fassett, C. I., & Head III, J. W. (2008). Valley network-fed, open-basin lakes on Mars:
 928 Distribution and implications for Noachian surface and subsurface
 929 hydrology. *Icarus*, 198(1), 37-56.
- 930 Fastook, J. L., Head, J. W., Scanlon, K. E., Weiss, D. K., & Palumbo, A. M. (2021).
 931 Hellas Basin, Mars: A Model of Rim and Wall Glaciation in the Late Noachian
 932 and Predictions for Enhanced Flow, Basal Melting, Wet-Based Glaciation and
 933 Erosion, and Generation and Fate of Meltwater. In *52nd Lunar and Planetary*
 934 *Science Conference* (No. 2548, p. 1528).
- 935 Fastook, J. L., & Head, J. W. (2015). Glaciation in the Late Noachian Icy Highlands: Ice
 936 accumulation, distribution, flow rates, basal melting, and top-down melting rates
 937 and patterns. *Planetary and Space Science*, 106, 82-98.
- 938 Forget, F., Wordsworth, R., Millour, E., Madeleine, J. B., Kerber, L., Leconte, J., ... &
 939 Haberle, R. M. (2013). 3D modelling of the early martian climate under a denser
 940 CO₂ atmosphere: Temperatures and CO₂ ice clouds. *Icarus*, 222(1), 81-99.
- 941 Fowler, A. C., & Chapwanya, M. (2014). An instability theory for the formation of
 942 ribbed moraine, drumlins and mega-scale glacial lineations. *Proceedings of the*
 943 *Royal Society A: Mathematical, Physical and Engineering Sciences*, 470(2171),
 944 20140185.
- 945 Gallagher, C., & Balme, M. (2015). Eskers in a complete, wet-based glacial system in the
 946 Phlegra Montes region, Mars. *Earth and Planetary Science Letters*, 431, 96-109.
- 947 Ghatan, G. J., & Head III, J. W. (2004). Regional drainage of meltwater beneath a
 948 Hesperian-aged south circumpolar ice sheet on Mars. *Journal of Geophysical*
 949 *Research: Planets*, 109(E7).
- 950 Ghatan, G. J., & Head III, J. W. (2002). Candidate subglacial volcanoes in the south polar
 951 region of Mars: Morphology, morphometry, and eruption conditions. *Journal of*
 952 *Geophysical Research: Planets*, 107(E7), 2-1.
- 953 Ghatan, G. J., Head III, J. W., & Pratt, S. (2003). Cavi Angusti, Mars: characterization
 954 and assessment of possible formation mechanisms. *Journal of Geophysical*
 955 *Research: Planets*, 108(E5).

- 956 Glavin, D. P., Freissinet, C., Miller, K. E., Eigenbrode, J. L., Brunner, A. E., Buch, A., ...
957 & Mahaffy, P. R. (2013). Evidence for perchlorates and the origin of chlorinated
958 hydrocarbons detected by SAM at the Rocknest aeolian deposit in Gale
959 Crater. *Journal of Geophysical Research: Planets*, 118(10), 1955-1973.
- 960 Goudge, T. A., Aureli, K. L., Head, J. W., Fassett, C. I., & Mustard, J. F. (2015).
961 Classification and analysis of candidate impact crater-hosted closed-basin lakes
962 on Mars. *Icarus*, 260, 346-367.
- 963 Grau Galofre, A., Whipple, K. X., Christensen, P. R., & Conway, S. J. (2022). Valley
964 networks and the record of glaciation on ancient Mars. *Geophysical research
965 letters*, 49(14), e2022GL097974.
- 966 Grau Galofre, A., Jellinek, A. M., & Osinski, G. R. (2020). Valley formation on early
967 Mars by subglacial and fluvial erosion. *Nature Geoscience*, 13(10), 663-668.
- 968 Galofre, A. G., Bahia, R. S., Jellinek, A. M., Whipple, K. X., & Gallo, R. (2020). Did
969 Martian valley networks substantially modify the landscape?. *Earth and
970 Planetary Science Letters*, 547, 116482.
- 971 Grimm, R. E., Harrison, K. P., Stillman, D. E., & Kirchoff, M. R. (2017). On the secular
972 retention of ground water and ice on Mars. *Journal of Geophysical Research:
973 Planets*, 122(1), 94-109.
- 974 Grott, M., Hauber, E., Werner, S. C., Kronberg, P., & Neukum, G. (2005). High heat flux
975 on ancient Mars: Evidence from rift flank uplift at Coracis Fossae. *Geophysical
976 Research Letters*, 32(21).
- 977 Guidat, T., Pochat, S., Bourgeois, O., & Souček, O. (2015). Landform assemblage in
978 Isidis Planitia, Mars: Evidence for a 3 Ga old polythermal ice sheet. *Earth and
979 Planetary Science Letters*, 411, 253-267.
- 980 Gulick, V. C. (1998). Magmatic intrusions and a hydrothermal origin for fluvial valleys
981 on Mars. *Journal of Geophysical Research: Planets*, 103(E8), 19365-19387.
- 982 Gulick, V. C. (2001). Origin of the valley networks on Mars: A hydrological
983 perspective. *Geomorphology*, 37(3-4), 241-268.
- 984 Guzewich, S. D., Way, M. J., Aleinov, I., Wolf, E. T., Del Genio, A., Wordsworth, R., &
985 Tsigaridis, K. (2021). 3D Simulations of the Early Martian Hydrological Cycle
986 Mediated by a H₂-CO₂ Greenhouse. *Journal of Geophysical Research:
987 Planets*, 126(7), e2021JE006825.
- 988 Haberle, R. M., Zahnle, K., Barlow, N. G., & Steakley, K. E. (2019). Impact degassing of
989 H₂ on early Mars and its effect on the climate system. *Geophysical Research
990 Letters*, 46(22), 13355-13362.
- 991 Halevy, I., Zuber, M. T., & Schrag, D. P. (2007). A sulfur dioxide climate feedback on
992 early Mars. *Science*, 318(5858), 1903-1907.
- 993 Harbor, J. M., Hallet, B., & Raymond, C. F. (1988). A numerical model of landform
994 development by glacial erosion. *Nature*, 333(6171), 347-349.
- 995 Hartmann, W. K., & Neukum, G. (2001). Cratering chronology and the evolution of
996 Mars. *Chronology and evolution of Mars*, 165-194.
- 997 Head III, J. W., & Pratt, S. (2001). Extensive Hesperian-aged south polar ice sheet on
998 Mars: Evidence for massive melting and retreat, and lateral flow and ponding of
999 meltwater. *Journal of Geophysical Research: Planets*, 106(E6), 12275-12299.

- 1000 Head, J., Forget, F., Wordsworth, R., Turbet, M., Cassanelli, J., & Palumbo, A. (2018).
 1001 Two oceans on Mars?: History, problems and prospects. In *The Ninth Moscow*
 1002 *Solar System Symposium 9M-S3* (pp. 15-18).
- 1003 Head, J. W., Nahm, A. L., Marchant, D. R., & Neukum, G. (2006). Modification of the
 1004 dichotomy boundary on Mars by Amazonian mid-latitude regional
 1005 glaciation. *Geophysical Research Letters*, 33(8).
- 1006 Head, J. W., Marchant, D. R., Agnew, M. C., Fassett, C. I., & Kreslavsky, M. A. (2006).
 1007 Extensive valley glacier deposits in the northern mid-latitudes of Mars: Evidence
 1008 for Late Amazonian obliquity-driven climate change. *Earth and Planetary*
 1009 *Science Letters*, 241(3-4), 663-671.
- 1010 Hecht, M. H., Kounaves, S. P., Quinn, R. C., West, S. J., Young, S. M., Ming, D. W., ...
 1011 & Smith, P. H. (2009). Detection of perchlorate and the soluble chemistry of
 1012 martian soil at the Phoenix lander site. *Science*, 325(5936), 64-67.
- 1013 Helgason, J. (1999). Formation of Olympus Mons and the aureole-escarpment problem
 1014 on Mars. *Geology*, 27(3), 231-234.
- 1015 Hiesinger, H., & Head III, J. W. (2002). Topography and morphology of the Argyre
 1016 Basin, Mars: implications for its geologic and hydrologic history. *Planetary and*
 1017 *Space Science*, 50(10-11), 939-981.
- 1018 Hobbs, P. V. (1974). *Ice Physics*, pp. (837-853), Clarendon.
- 1019 Ann Hodges, C., & Moore, H. J. (1979). The subglacial birth of Olympus Mons and its
 1020 aureoles. *Journal of Geophysical Research: Solid Earth*, 84(B14), 8061-8074.
- 1021 Howard, A. D. (1981). Etched plains and braided ridges of the south polar region of
 1022 Mars: Features produced by basal melting of ground ice?. *Reports of Planetary*
 1023 *Geology Program*, 286-288.
- 1024 Howard, A. D., Moore, J. M., & Irwin III, R. P. (2005). An intense terminal epoch of
 1025 widespread fluvial activity on early Mars: 1. Valley network incision and
 1026 associated deposits. *Journal of Geophysical Research: Planets*, 110(E12).
- 1027 Hynek, B. M., Beach, M., & Hoke, M. R. (2010). Updated global map of Martian valley
 1028 networks and implications for climate and hydrologic processes. *Journal of*
 1029 *Geophysical Research: Planets*, 115(E9).
- 1030 Irwin III, R. P., Howard, A. D., Craddock, R. A., & Moore, J. M. (2005). An intense
 1031 terminal epoch of widespread fluvial activity on early Mars: 2. Increased runoff
 1032 and paleolake development. *Journal of Geophysical Research: Planets*, 110(E12).
- 1033 Irwin III, R. P., Craddock, R. A., Howard, A. D., & Flemming, H. L. (2011).
 1034 Topographic influences on development of Martian valley networks. *Journal of*
 1035 *Geophysical Research: Planets*, 116(E2).
- 1036 Irwin III, R. P., Wray, J. J., Mest, S. C., & Maxwell, T. A. (2018). Wind-eroded crater
 1037 floors and intercrater plains, Terra Sabaea, Mars. *Journal of Geophysical*
 1038 *Research: Planets*, 123(2), 445-467.
- 1039 Ivanov, M. A., Hiesinger, H., Erkeling, G., Hielscher, F. J., & Reiss, D. (2012). Major
 1040 episodes of geologic history of Isidis Planitia on Mars. *Icarus*, 218(1), 24-46.
- 1041 Jakosky, B. M. (2021). Atmospheric loss to space and the history of water on
 1042 Mars. *Annual Review of Earth and Planetary Sciences*, 49, 71-93.
- 1043 Johnson, S. S., Mischna, M. A., Grove, T. L., & Zuber, M. T. (2008). Sulfur-induced
 1044 greenhouse warming on early Mars. *Journal of Geophysical Research:*
 1045 *Planets*, 113(E8).

- 1046 Kamada, A., Kuroda, T., Kasaba, Y., Terada, N., Nakagawa, H., & Toriumi, K. (2020). A
1047 coupled atmosphere–hydrosphere global climate model of early Mars: A ‘cool
1048 and wet’ scenario for the formation of water channels. *Icarus*, 338, 113567.
- 1049 Kargel, J. S., & Strom, R. G. (1992). Ancient glaciation on Mars. *Geology*, 20(1), 3-7.
- 1050 Kerber, L., Forget, F., & Wordsworth, R. (2015). Sulfur in the early martian atmosphere
1051 revisited: Experiments with a 3-D Global Climate Model. *Icarus*, 261, 133-148.
- 1052 Kite, E. S. (2019). Geologic constraints on early Mars climate. *Space Science
1053 Reviews*, 215(1), 1-47.
- 1054 Kite, E. S., & Daswani, M. M. (2019). Geochemistry constrains global hydrology on
1055 Early Mars. *Earth and Planetary Science Letters*, 524, 115718.
- 1056 Kite, E. S., & Hindmarsh, R. C. (2007). Did ice streams shape the largest channels on
1057 Mars?. *Geophysical Research Letters*, 34(19).
- 1058 Kite, E. S., Matsuyama, I., Manga, M., Perron, J. T., & Mitrovica, J. X. (2009). True
1059 Polar Wander driven by late-stage volcanism and the distribution of paleopolar
1060 deposits on Mars. *Earth and Planetary Science Letters*, 280(1-4), 254-267.
- 1061 Kite, E. S., Williams, J. P., Lucas, A., & Aharonson, O. (2014). Low palaeopressure of
1062 the Martian atmosphere estimated from the size distribution of ancient
1063 craters. *Nature Geoscience*, 7(5), 335-339.
- 1064 Kounaves, S. P., Carrier, B. L., O’Neil, G. D., Stroble, S. T., & Claire, M. W. (2014).
1065 Evidence of martian perchlorate, chlorate, and nitrate in Mars meteorite
1066 EETA79001: Implications for oxidants and organics. *Icarus*, 229, 206-213.
- 1067 Koutnik, M., Butcher, F., Soare, R., Hepburn, A., Hubbard, B., Brough, B., Gallagher, C.,
1068 McKeown, L. & Pathare, A. (2023). Glacial Deposits, Remnants and Landscapes
1069 on Amazonian Mars: Using setting, structure, and stratigraphy to understand ice
1070 evolution and climate history. In *Ice across the Solar System* (pp. X-X). Elsevier.
- 1071 Kress, A. M., & Head, J. W. (2015). Late Noachian and early Hesperian ridge systems in
1072 the south circumpolar Dorsa Argentea Formation, Mars: Evidence for two stages
1073 of melting of an extensive late Noachian ice sheet. *Planetary and Space
1074 Science*, 109, 1-20.
- 1075 Kreslavsky, M. A., & Head, J. W. (2018). Mars climate history: Insights from impact
1076 crater wall slope statistics. *Geophysical Research Letters*, 45(4), 1751-1758.
- 1077 Lamb, M. P., Howard, A. D., Johnson, J., Whipple, K. X., Dietrich, W. E., & Perron, J.
1078 T. (2006). Can springs cut canyons into rock?. *Journal of Geophysical Research:
1079 Planets*, 111(E7).
- 1080 Laskar, J., Correia, A. C. M., Gastineau, M., Joutel, F., Levrard, B., & Robutel, P. (2004).
1081 Long term evolution and chaotic diffusion of the insolation quantities of
1082 Mars. *Icarus*, 170(2), 343-364.
- 1083 Lasue, J., Mangold, N., Hauber, E., Clifford, S., Feldman, W., Gasnault, O., ... & Mosis,
1084 O. (2013). Quantitative assessments of the martian hydrosphere. *Space Science
1085 Reviews*, 174(1), 155-212.
- 1086 Lee, P., Rice Jr, J. W., Bunch, T. E., Grieve, R. A. F., McKay, C. P., Schutt, J. W., &
1087 Zent, A. P. (1999, January). Possible analogs for small valleys on Mars at the
1088 Haughton impact crater site, Devon Island, Canadian High Arctic. In *Lunar and
1089 Planetary Science*.
- 1090 Lopes, R., Guest, J. E., & Wilson, C. J. (1980). Origin of the Olympus Mons aureole and
1091 perimeter scarp. *The moon and the planets*, 22(2), 221-234.

- 1092 Lucchitta, B. K. (2001). Antarctic ice streams and outflow channels on
 1093 Mars. *Geophysical Research Letters*, 28(3), 403-406.
- 1094 Lucchitta, B. K., & Ferguson, H. M. (1983). Chryse Basin channels: Low-gradients and
 1095 ponded flows. *Journal of Geophysical Research: Solid Earth*, 88(S02), A553-
 1096 A568.
- 1097 Malin, M. C., & Carr, M. H. (1999). Groundwater formation of Martian
 1098 valleys. *Nature*, 397(6720), 589-591.
- 1099 Manga, M., & Wright, V. (2021). No Cryosphere-Confined Aquifer Below InSight on
 1100 Mars. *Geophysical Research Letters*, 48(8), e2021GL093127.
- 1101 Manga, M., Patel, A., Dufek, J., & Kite, E. S. (2012). Wet surface and dense atmosphere
 1102 on early Mars suggested by the bomb sag at Home Plate, Mars. *Geophysical
 1103 Research Letters*, 39(1).
- 1104 Manning, C. E., & Ingebritsen, S. E. (1999). Permeability of the continental crust:
 1105 Implications of geothermal data and metamorphic systems. *Reviews of
 1106 Geophysics*, 37(1), 127-150.
- 1107 Marinova, M. M., Aharonson, O., & Asphaug, E. (2008). Mega-impact formation of the
 1108 Mars hemispheric dichotomy. *Nature*, 453(7199), 1216-1219.
- 1109 Martínez-Alonso, S., Mellon, M. T., Banks, M. E., Keszthelyi, L. P., McEwen, A. S., &
 1110 Team, T. H. (2011). Evidence of volcanic and glacial activity in Chryse and
 1111 Acidalia Planitiae, Mars. *Icarus*, 212(2), 597-621.
- 1112 Matherne, C., Skok, J. R., Mustard, J. F., Karunatillake, S., & Doran, P. (2020).
 1113 Multistage ice-damming of volcanic flows and fluvial systems in Northeast Syrtis
 1114 Major. *Icarus*, 340, 113608.
- 1115 McGovern, P. J., Solomon, S. C., Smith, D. E., Zuber, M. T., Simons, M., Wieczorek, M. A., ... & Head, J. W. (2002). Localized
 1116 gravity/topography admittance and correlation spectra on Mars: Implications for
 1117 regional and global evolution. *Journal of Geophysical Research:
 1118 Planets*, 107(E12), 19-1.
- 1119 McGovern, P. J., Solomon, S. C., Smith, D. E., Zuber, M. T., Simons, M., Wieczorek, M.
 1120 A., ... & Head, J. W. (2004). Correction to “Localized gravity/topography
 1121 admittance and correlation spectra on Mars: Implications for regional and global
 1122 evolution”. *Journal of Geophysical Research: Planets*, 109(E7).
- 1123 McLennan, S. M., Grotzinger, J. P., Hurowitz, J. A., & Tosca, N. J. (2019). The
 1124 sedimentary cycle on early Mars. *Annual Review of Earth and Planetary
 1125 Sciences*, 47, 91-118.
- 1126 Milkovich, S. M., Head III, J. W., & Pratt, S. (2002). Meltback of Hesperian-aged ice-
 1127 rich deposits near the south pole of Mars: Evidence for drainage channels and
 1128 lakes. *Journal of Geophysical Research: Planets*, 107(E6), 10-1.
- 1129 Mischna, M. A., Baker, V., Milliken, R., Richardson, M., & Lee, C. (2013). Effects of
 1130 obliquity and water vapor/trace gas greenhouses in the early martian
 1131 climate. *Journal of Geophysical Research: Planets*, 118(3), 560-576.
- 1132 Montgomery, D. R., Som, S. M., Jackson, M. P., Schreiber, B. C., Gillespie, A. R., &
 1133 Adams, J. B. (2009). Continental-scale salt tectonics on Mars and the origin of
 1134 Valles Marineris and associated outflow channels. *Geological Society of America
 1135 Bulletin*, 121(1-2), 117-133.
- 1136 Morgan, G. A., Head III, J. W., & Marchant, D. R. (2009). Lineated valley fill (LVF) and
 1137 lobate debris aprons (LDA) in the Deuteronilus Mensae northern dichotomy

- 1138 boundary region, Mars: Constraints on the extent, age and episodicity of
 1139 Amazonian glacial events. *Icarus*, 202(1), 22-38.
- 1140 Mustard, J. F., Cooper, C. D., & Rifkin, M. K. (2001). Evidence for recent climate
 1141 change on Mars from the identification of youthful near-surface ground
 1142 ice. *Nature*, 412(6845), 411-414.
- 1143 Neukum, G., Basilevsky, A. T., Kneissl, T., Chapman, M. G., Van Gasselt, S., Michael,
 1144 G., ... & Lanz, J. K. (2010). The geologic evolution of Mars: Episodicity of
 1145 resurfacing events and ages from cratering analysis of image data and correlation
 1146 with radiometric ages of Martian meteorites. *Earth and Planetary Science
 1147 Letters*, 294(3-4), 204-222.
- 1148 Ojha, L., Buffo, J., Karunatillake, S., & Siegler, M. (2020). Groundwater production from
 1149 geothermal heating on early Mars and implication for early martian
 1150 habitability. *Science advances*, 6(49), eabb1669.
- 1151 Palumbo, A. M., & Head, J. W. (2019). Oceans on Mars: The possibility of a Noachian
 1152 groundwater-fed ocean in a sub-freezing martian climate. *Icarus*, 331, 209-225.
- 1153 Palumbo, A. M., & Head, J. W. (2020). Groundwater release on early Mars: Utilizing
 1154 models and proposed evidence for groundwater release to estimate the required
 1155 climate and subsurface water budget. *Geophysical Research Letters*, 47(8),
 1156 e2020GL087230.
- 1157 Pan, L., Ehlmann, B. L., Carter, J., & Ernst, C. M. (2017). The stratigraphy and history of
 1158 Mars' northern lowlands through mineralogy of impact craters: A comprehensive
 1159 survey. *Journal of Geophysical Research: Planets*, 122(9), 1824-1854.
- 1160 Parker, T. J., Saunders, R. S., & Schneeberger, D. M. (1989). Transitional morphology in
 1161 west Deuteronilus Mensae, Mars: Implications for modification of the
 1162 lowland/upland boundary. *Icarus*, 82(1), 111-145.
- 1163 Penido, J. C., Fassett, C. I., & Som, S. M. (2013). Scaling relationships and concavity of
 1164 small valley networks on Mars. *Planetary and Space Science*, 75, 105-116.
- 1165 Perron, J. T., Mitrovica, J. X., Manga, M., Matsuyama, I., & Richards, M. A. (2007).
 1166 Evidence for an ancient martian ocean in the topography of deformed
 1167 shorelines. *Nature*, 447(7146), 840-843.
- 1168 Phillips, R. J., Zuber, M. T., Solomon, S. C., Golombek, M. P., Jakosky, B. M., Banerdt,
 1169 W. B., ... & Hauck II, S. A. (2001). Ancient geodynamics and global-scale
 1170 hydrology on Mars. *Science*, 291(5513), 2587-2591.
- 1171 Plaut, J. J., Safaeinili, A., Holt, J. W., Phillips, R. J., Head III, J. W., Seu, R., Putzig, N.E.
 1172 & Frigeri, A. (2009). Radar evidence for ice in lobate debris aprons in the mid-
 1173 northern latitudes of Mars. *Geophysical research letters*, 36(2).
- 1174 Plesa, A. C., Grott, M., Tosi, N., Breuer, D., Spohn, T., & Wieczorek, M. A. (2016). How
 1175 large are present-day heat flux variations across the surface of Mars?. *Journal of
 1176 Geophysical Research: Planets*, 121(12), 2386-2403.
- 1177 Rao, M. N., Sutton, S. R., McKay, D. S., & Dreibus, G. (2005). Clues to Martian brines
 1178 based on halogens in salts from nakhlites and MER samples. *Journal of
 1179 Geophysical Research: Planets*, 110(E12).
- 1180
- 1181 Rao, M. N., Nyquist, L. E., Wentworth, S. J., Sutton, S. R., & Garrison, D. H. (2008).
 1182 The nature of Martian fluids based on mobile element studies in salt-assemblages
 1183 from Martian meteorites. *Journal of Geophysical Research: Planets*, 113(E6).

- 1184 Ramirez, R. M., & Craddock, R. A. (2018). The geological and climatological case for a
 1185 warmer and wetter early Mars. *Nature Geoscience*, *11*(4), 230-237.
- 1186 Read, P. L., & Lewis, S. R. (2004). *The Martian climate revisited: atmosphere and*
 1187 *environment of a desert planet*. Springer Science & Business Media.
- 1188 Robbins, S. J., Hynek, B. M., Lillis, R. J., & Bottke, W. F. (2013). Large impact crater
 1189 histories of Mars: The effect of different model crater age
 1190 techniques. *Icarus*, *225*(1), 173-184.
- 1191 Rodriguez, J. A. P., Fairén, A. G., Tanaka, K. L., Zarroca, M., Linares, R., Platz, T., ... &
 1192 Glines, N. (2016). Tsunami waves extensively resurfaced the shorelines of an
 1193 early Martian ocean. *Scientific reports*, *6*(1), 1-8.
- 1194 Scanlon, K. E., Head, J. W., Fastook, J. L., & Wordsworth, R. D. (2018). The Dorsa
 1195 Argentea formation and the Noachian-Hesperian climate transition. *Icarus*, *299*,
 1196 339-363.
- 1197 Scanlon, K. E. (2016). Ice sheet melting throughout Mars climate history: Mechanisms,
 1198 rates, and implications. *Ph. D. Thesis*.
- 1199 Schmidt, F., Way, M. J., Costard, F., Bouley, S., Séjourné, A., & Aleinov, I. (2022).
 1200 Circumpolar ocean stability on Mars 3 Gy ago. *Proceedings of the National*
 1201 *Academy of Sciences*, *119*(4), e2112930118.
- 1202 Schwenzer, S. P., Abramov, O., Allen, C. C., Clifford, S. M., Cockell, C. S., Filiberto, J.,
 1203 ... & Wiens, R. C. (2012). Puncturing Mars: How impact craters interact with the
 1204 Martian cryosphere. *Earth and Planetary Science Letters*, *335*, 9-17.
- 1205 Smith, D. E., Zuber, M. T., Frey, H. V., Garvin, J. B., Head, J. W., Muhleman, D. O., ...
 1206 & Sun, X. (2001). Mars Orbiter Laser Altimeter: Experiment summary after the
 1207 first year of global mapping of Mars. *Journal of Geophysical Research:*
 1208 *Planets*, *106*(E10), 23689-23722.
- 1209 Smith, D., Neumann, G., Arvidson, R. E., Guinness, E. A., & Slavney, S. (2003). Mars
 1210 Global Surveyor laser altimeter mission experiment gridded data record. *NASA*
 1211 *Planetary Data System*.
- 1212 Som, S. M., Montgomery, D. R., & Greenberg, H. M. (2009). Scaling relations for large
 1213 Martian valleys. *Journal of Geophysical Research: Planets*, *114*(E2).
- 1214 Souček, O., Bourgeois, O., Pochat, S., & Guidat, T. (2015). A 3 Ga old polythermal ice
 1215 sheet in Isidis Planitia, Mars: Dynamics and thermal regime inferred from
 1216 numerical modeling. *Earth and Planetary Science Letters*, *426*, 176-190.
- 1217 Šrámek, O., & Zhong, S. (2012). Martian crustal dichotomy and Tharsis formation by
 1218 partial melting coupled to early plume migration. *Journal of Geophysical*
 1219 *Research: Planets*, *117*(E1).
- 1220 Steakley, K., Murphy, J., Kahre, M., Haberle, R., & Kling, A. (2019). Testing the impact
 1221 heating hypothesis for early Mars with a 3-D global climate model. *Icarus*, *330*,
 1222 169-188.
- 1223 Storrar, R. D., Stokes, C. R., & Evans, D. J. (2013). A map of large Canadian eskers from
 1224 Landsat satellite imagery. *Journal of maps*, *9*(3), 456-473.
- 1225 Storrar, R. D., Stokes, C. R., & Evans, D. J. (2014). Morphometry and pattern of a large
 1226 sample (> 20,000) of Canadian eskers and implications for subglacial drainage
 1227 beneath ice sheets. *Quaternary Science Reviews*, *105*, 1-25.
- 1228 Storrar, R. D., Evans, D. J., Stokes, C. R., & Ewertowski, M. (2015). Controls on the
 1229 location, morphology and evolution of complex esker systems at decadal

- 1230 timescales, Breiðamerkurjökull, southeast Iceland. *Earth Surface Processes and*
 1231 *Landforms*, 40(11), 1421-1438.
- 1232 Svendsen, J. I., Alexanderson, H., Astakhov, V. I., Demidov, I., Dowdeswell, J. A.,
 1233 Funder, S., ... & Stein, R. (2004). Late Quaternary ice sheet history of northern
 1234 Eurasia. *Quaternary Science Reviews*, 23(11-13), 1229-1271.
- 1235 Tanaka, K. L. (1985). Ice-lubricated gravity spreading of the Olympus Mons aureole
 1236 deposits. *Icarus*, 62(2), 191-206.
- 1237 Tanaka, K. L., Robbins, S. J., Fortezzo, C. M., Skinner Jr, J. A., & Hare, T. M. (2014).
 1238 The digital global geologic map of Mars: Chronostratigraphic ages, topographic
 1239 and crater morphologic characteristics, and updated resurfacing history. *Planetary*
 1240 *and Space Science*, 95, 11-24.
- 1241 Turbet, M., Forget, F., Head, J. W., & Wordsworth, R. (2017). 3D modelling of the
 1242 climatic impact of outflow channel formation events on early Mars. *Icarus*, 288,
 1243 10-36.
- 1244 Urata, R. A., & Toon, O. B. (2013). Simulations of the martian hydrologic cycle with a
 1245 general circulation model: Implications for the ancient martian
 1246 climate. *Icarus*, 226(1), 229-250.
- 1247 Villanueva, G. L., Mumma, M. J., Novak, R. E., Käufl, H. U., Hartogh, P., Encrenaz, T.,
 1248 ... & Smith, M. D. (2015). Strong water isotopic anomalies in the martian
 1249 atmosphere: Probing current and ancient reservoirs. *Science*, 348(6231), 218-221.
- 1250 Ward, W. R., Burns, J. A., & Toon, O. B. (1979). Past obliquity oscillations of Mars: The
 1251 role of the Tharsis uplift. *Journal of Geophysical Research: Solid Earth*, 84(B1),
 1252 243-259.
- 1253 Warren, A. O., Kite, E. S., Williams, J. P., & Horgan, B. (2019). Through the thick and
 1254 thin: New constraints on Mars paleopressure history 3.8–4 Ga from small
 1255 exhumed craters. *Journal of Geophysical Research: Planets*, 124(11), 2793-2818.
- 1256 Weiss, D. K., & Head, J. W. (2017). Evidence for stabilization of the ice-cemented
 1257 cryosphere in earlier Martian history: Implications for the current abundance of
 1258 groundwater at depth on Mars. *Icarus*, 288, 120-147.
- 1259 Weiss, D. K., & Head, J. W. (2015). Crater degradation in the Noachian highlands of
 1260 Mars: Assessing the hypothesis of regional snow and ice deposits on a cold and
 1261 icy early Mars. *Planetary and Space Science*, 117, 401-420.
- 1262 Weiss, D. K., & Head, J. W. (2017). Salt or ice diapirism origin for the honeycomb
 1263 terrain in Hellas basin, Mars?: Implications for the early martian
 1264 climate. *Icarus*, 284, 249-263.
- 1265 Werner, S. C. (2009). The global martian volcanic evolutionary history. *Icarus*, 201(1),
 1266 44-68.
- 1267 Wordsworth, R., Ehlmann, B., Forget, F., Haberle, R., Head, J., & Kerber, L. (2018).
 1268 Healthy debate on early Mars. *Nature Geoscience*, 11(12), 888-888.
- 1269 Wordsworth, R., Forget, F., Millour, E., Madeleine, J. B., Charnay, B., & Haberle, R.
 1270 (2011). Modelling past Mars Climates and water cycle with a thicker CO₂
 1271 atmosphere. *Mars Atmosphere: Modelling and Observation*, 447-448.
- 1272 Wordsworth, R. D. (2016). The climate of early Mars. *Annual Review of Earth and*
 1273 *Planetary Sciences*, 44, 381-408.
- 1274 Wordsworth, R. D., Kerber, L., Pierrehumbert, R. T., Forget, F., & Head, J. W. (2015).
 1275 Comparison of “warm and wet” and “cold and icy” scenarios for early Mars in a

- 1276 3-D climate model. *Journal of Geophysical Research: Planets*, 120(6), 1201-
1277 1219.
- 1278 Wordsworth, R., Knoll, A. H., Hurowitz, J., Baum, M., Ehlmann, B. L., Head, J. W., &
1279 Steakley, K. (2021). A coupled model of episodic warming, oxidation and
1280 geochemical transitions on early Mars. *Nature Geoscience*, 14(3), 127-132.
- 1281 Wordsworth, R., Forget, F., Millour, E., Head, J. W., Madeleine, J. B., & Charnay, B.
1282 (2013). Global modelling of the early martian climate under a denser CO2
1283 atmosphere: Water cycle and ice evolution. *Icarus*, 222(1), 1-19.
- 1284 Wordsworth, R., Kalugina, Y., Lokshtanov, S., Vigasin, A., Ehlmann, B., Head, J., ... &
1285 Wang, H. (2017). Transient reducing greenhouse warming on early
1286 Mars. *Geophysical Research Letters*, 44(2), 665-671.
- 1287 Yin, A., Moon, S., & Day, M. (2021). Landform evolution of Oudemans crater and its
1288 bounding plateau plains on Mars: Geomorphological constraints on the Tharsis
1289 ice-cap hypothesis. *Icarus*, 360, 114332.
- 1290 Zealey, W. J. (2009). Glacial, periglacial and glacio-volcanic structures on the Echus
1291 Plateau, upper Kasei Valles. *Planetary and Space Science*, 57(5-6), 699-710.